

University of Nebraska - Lincoln

DigitalCommons@University of Nebraska - Lincoln

Biological Systems Engineering--Dissertations,
Theses, and Student Research

Biological Systems Engineering

12-2018

Variable Rate Irrigation Using a Spatial Evapotranspiration Model With Remote Sensing Imagery and Soil Water Content Measurements

Sandeep Bhatti

University of Nebraska-Lincoln, sandeep.bhatti@huskers.unl.edu

Follow this and additional works at: <http://digitalcommons.unl.edu/biosysengdiss>



Part of the [Bioresource and Agricultural Engineering Commons](#)

Bhatti, Sandeep, "Variable Rate Irrigation Using a Spatial Evapotranspiration Model With Remote Sensing Imagery and Soil Water Content Measurements" (2018). *Biological Systems Engineering--Dissertations, Theses, and Student Research*. 83.
<http://digitalcommons.unl.edu/biosysengdiss/83>

This Article is brought to you for free and open access by the Biological Systems Engineering at DigitalCommons@University of Nebraska - Lincoln. It has been accepted for inclusion in Biological Systems Engineering--Dissertations, Theses, and Student Research by an authorized administrator of DigitalCommons@University of Nebraska - Lincoln.

VARIABLE RATE IRRIGATION USING A SPATIAL EVAPOTRANSPIRATION
MODEL WITH SATELLITE AND UNMANNED AERIAL SYSTEMS IMAGERY
AND SOIL WATER CONTENT MEASUREMENTS

by

Sandeep Bhatti

A THESIS

Presented to the Faculty of
The Graduate College at the University of Nebraska
In Partial Fulfillment of Requirements
For the Degree of Master of Science

Major: Agricultural and Biological Systems Engineering

Under the Supervision of Professor Derek M. Heeren

Lincoln, Nebraska

December, 2018

VARIABLE RATE IRRIGATION USING A SPATIAL EVAPOTRANSPIRATION
MODEL WITH REMOTE SENSING IMAGERY AND SOIL WATER CONTENT
MEASUREMENTS

Sandeep Bhatti, M.S.

University of Nebraska, 2018

Advisor: Derek M. Heeren

Site-specific variable rate irrigation (VRI) may help in intensification of agriculture by producing more yield per unit of land and water. VRI could be managed using different methods. Real time spatial information about water balance components is important for designing VRI prescription maps. This work involved use of a spatial evapotranspiration (*ET*) model for studying spatial variability in an agricultural field at the Eastern Nebraska Research and Extension Center near Mead, Nebraska. Imagery from unmanned aerial systems (UASs) and Landsat were used as input for the spatial evapotranspiration model. Other inputs into the model were soil water content measurements from neutron probes, weather data, crop data, previous irrigation prescriptions, and soil properties for the field. Weekly prescriptions were output from the model and were applied to respective VRI treatments. The work included comparison of VRI treatments with uniform irrigation and rainfed treatments in terms of yield potential and reduced water withdrawal. Uniform irrigation methods included uniform irrigation managed using soil water content measurements from neutron probe and rainfed treatment. The objectives were to quantify benefits of VRI in terms of crop yield and

consumptive use. Other water balance variables were also compared among the treatments. The model was updated and improved during the study period in attempt to more accurately model water balance components and manage VRI. One addition to the model was a decaying method of modeling deep percolation allowing soil water content to exceed field capacity temporarily after a wetting event. Treatment differences were tested at 5% significance for yield and irrigation results. Mean total prescribed irrigation depth was significantly larger for VRI using Landsat than uniform treatments for soybean in 2017. It was significantly lower for VRI using Landsat than other irrigated treatments for soybean in 2018. No other differences in applied irrigation depth were found between treatments. Maize yield in 2017 was significantly greater for VRI using Landsat and uniform treatments than the rainfed treatment. No other significant yield differences were observed in 2017 and 2018. The VRI-L and uniform treatments performed better than rainfed for maize in 2017 by significantly increasing maize yield due to irrigation. VRI-L treatment in 2018 was managed using less water for soybean showing reduction in water withdrawal over other irrigated treatments. Hence, VRI-L performed well in these cases. VRI-U treatment performed similar to uniform treatment in 2018. Future research may focus on: 1) inclusion of thermal infrared UAS imagery in the model to detect stress, 2) development of a more advanced method of incorporating water content measurements in the model, and 3) more research on managing VRI using UAS imagery at commercial field scales.

ACKNOWLEDGEMENTS

I would like to express my sincere and utmost gratitude to those who have inspired and supported me in completing my research. I am indebted to their contribution in the research, study, and inputs for this thesis.

First and foremost, I would like to thank God for providing me with the opportunity, strength, and perseverance to undertake this research study and complete it successfully.

This thesis has been completed with the support and guidance of many individuals. I apologize in advance if I missed names of those that contributed to my research. I am truly indebted for their contribution in the research, study, and inputs for this thesis. I found an inspiration, a guide, a teacher, a mentor, and a true friend in my advisor Dr. Derek Heeren. His guidance, patience, and knowledge have been invaluable and a key piece of my research. He has given me the freedom to pursue my research and yet encouraged me to think critically about each component of my study. Without his guidance, this thesis would not have been possible and I shall eternally be grateful to him for his assistance and mentorship.

I owe a debt of gratitude to my thesis committee which includes: Dr. Christopher Neale, Dr. Wayne Woldt, and Dr. Daran Rudnick. Thank you all for your invaluable advice and for always being so supportive of my work. I believe my thesis would not be as successful if it were not for Dr. Burdette Barker. From teaching me the model to helping me understand the basic and crucial components of my research methodology, thank you for always providing me with constructive feedback, time, energy, and your extensive expertise since the beginning.

I would like to give special thanks to Mr. Alan Boldt who has helped me tremendously in the lab as well as in the field. The amount of time he has spent to provide his knowledge and input has been invaluable throughout my research. I am truly grateful for his contributions towards my research.

I express my sincere gratitude to the personnel such as Mr. Mark Schroeder, Mr. Mike Murren, Mr. Blaine Clowser, Mr. Nathan Thorson, Mr. Keith Stewart, and others of the University of Nebraska's Eastern Nebraska Research and Extension Center for providing accommodations through monitoring the crops and performing the farm operations. I would also like to thank Tyler Smith and Ms. Ronica Stromberg from the Biological Systems Engineering Department who aided in research related activities.

I could not have completed my research work without the support from my graduate and undergraduate fellows such as, Mitch Maguire, Tsz Him Lo, Troy Nelson, Isabella Possignolo, Tonny Ruhinda, Simbi Mvuyekure, Joviale Uwase, Julienne Irihose, Rene Francis, and Jasreman Singh. I must also thank Mitch Maguire, specifically, for collecting UAS imagery from the field which was used as an input to the model.

Throughout the project, data pertaining to the weather was provided by the High Plains Regional Climate Center. The U.S. Geological Survey was also used to retrieve Landsat satellite imagery.

I would like to thank funding sources, namely, Graduate Student Support from the Robert B. Daugherty Water for Food Global Institute at the University of Nebraska, a USGS 104(b) grant from the Nebraska Water Center, and a grant from the USDA National Institute of Food and Agriculture's Agricultural and Food Research Initiative (Award Number 2017-

67021-26249). Additional support was received from the Hatch Act (USDA NIFA, Accession Number 1009760) and the Department of Biological Systems Engineering at the University of Nebraska-Lincoln. Many thanks to those who awarded me travel and fellowship funding and various other awards. These included Farmer's National Company Fellowship 2018, David H. & Annie E. Larrick Student Travel Funds 2018, Elenore Gakemeier Swarts Graduate Student Travel Award 2018,

I will always be grateful for the endless support, the sacrifices, and unconditional love that has been given to me by my family. Thank you, from the bottom of my heart, for always encouraging me in all of my pursuits and inspiring me to follow my dreams.

TABLE OF CONTENTS

LIST OF TABLES	vii
LIST OF FIGURES	viii
CHAPTER 1. INTRODUCTION AND OBJECTIVES OF RESEARCH.....	1
1.1 Motivation for Study.....	1
1.2 Literature Review.....	2
1.2.1 VRI Management Factors	2
1.2.2 Remote Sensing in VRI	4
1.2.3 VRI Management Systems	6
1.2.4 Potential Benefits of Variable Rate Irrigation	9
1.2.5 Conclusion	10
1.3 Objectives	11
1.4 References.....	12
CHAPTER 2. PERFORMANCE OF VARIABLE RATE IRRIGATION MANAGEMENT USING A SPATIAL EVAPOTRANSPIRATION MODEL WITH SATELLITE AND AIRBORNE IMAGERY UPDATED USING SOIL WATER CONTENT MEASUREMENTS	17
Abstract.....	17
2.1 Introduction.....	18
2.2 Material and Methods	21
2.2.1 Study Site.....	21
2.2.2 Experimental Design.....	22

2.2.3 Acquired Data	25
2.2.4 Water Balance Components.....	29
2.2.5 SETMI Modeling for Irrigation Management	34
2.2.6 Data Analysis	37
2.3 Results and Discussion	40
2.3.1 Soil Properties	40
2.3.2 Rainfall.....	41
2.3.3 Remote Sensing Imagery	41
2.3.4 Eliminated Data	43
2.3.5 Mean Total Gross Prescribed Irrigation Depth.....	43
2.3.6 Correlation Among Response Variables.....	45
2.3.7 MANOVA and Univariate ANOVA Test Results.....	46
2.3.8 Modeling Differences using UAS and Landsat Imagery	53
2.3.9 Challenges in Using UAS Thermal Infrared Imagery in the TSEB Model	55
2.4 Summary and Conclusions	56
Acknowledgements.....	58
2.5 References:.....	59
CHAPTER 3. GENERAL OBSERVATIONS AND FUTURE WORK.....	64
3.1 Seasonal Depletion for Sample Plots in VRI and Uniform Treatments	64
3.2 Catch Can Test for System Evaluation	66
3.3 Future Direction and Recommendations	67
A. APPENDIX:.....	70

A.1 Modeling Accuracy Using the New Method of Deep Percolation Estimation	70
A.2 Spatial Variability in Depletion Among Plots	72
A.2 Tables and Figures	73

LIST OF TABLES

Table	Page
Table 2.1 List of dates of satellite imagery used in VRI-L treatment in 2017 and 2018..	42
Table 2.2. List of UAS images used in 2018.	42
Table 2.3. Mean total seasonal gross irrigation prescribed for treatments in 2017 and 2018.....	45
Table 2.4. Partial correlation coefficients for response variables.	45
Table 2.5. ANOVA test results for different response variables with least squares mean and multiple ranges groupings	48
Table 2.6. Different water use efficiencies for treatments for maize and soybean in 2017 and 2018.....	52
Table A.1. Comparison of two methods of simulating seasonal modeled depletion using measured depletion.	72
Table A.2. Summary of multivariate analysis of variance (MANOVA) tests using Wilks's Lambda Statistic in 2017 and 2018.....	75
Table A.3. Summary of univariate analysis of variance (ANOVA) tests for various response variables for all fields in 2017	75
Table A.4. Temperature (°C) of thermal imagery from UAS and temperature measurements from IRT for 29 date-locations in the field.	75

LIST OF FIGURES

Figure	Page
Figure 2.1 Plot layout of experiment in 2017 and 2018. Letters inside plots denote treatments applied in 2017/2018.....	24
Figure 2.2 Total mean prescribed irrigation depth for each plot in 2017 and 2018.	44
Figure 2.3. Dry yield for treatments for maize and soybean in 2017.	49
Figure 2.4. Computed SAVI using Landsat 8 imagery for experimental plots (green and yellow) with a Landsat 8 thermal infrared surface temperature image background.	53
Figure 2.5. Computed SAVI using UAS imagery for experimental plots (green and red) with a UAS thermal infrared surface temperature image background	54
Figure 3.1. Seasonal soil water depletion for a uniform plot for ENREC Maize in 2017. Maximum irrigation depth is shown by green dotted line taking reference to MAD (red line).....	65
Figure 3.2. Seasonal soil water depletion for a VRI plot for ENREC Maize in 2017. Maximum irrigation depth is shown by green dotted line taking reference to MAD (red line).....	65
Figure 3.3. Catch can layout (shown in dots) and irrigation prescription map for conducting end of season catch can evaluation in 2017.	67
Figure A.1. Seasonal depletion modeled using instantaneous and decaying deep percolation (DP) methods for one plot in soybean in 2017.	71
Figure A.2. Seasonal depletion for 3 plots in VRI-U for soybean in 2018.....	72
Figure A.3. Spatial maize yield (bu ac ⁻¹) at market moisture planted north of the field in 2017.	73

Figure A.4. Spatial soybean yield (bu ac ⁻¹) at market moisture in south of the field in 2017.	73
Figure A.5. Plot maize yield (bu ac ⁻¹) at market moisture planted north of the field in 2017.....	74
Figure A.6. Plot soybean yield (bu ac ⁻¹) at market moisture planted south of the field in 2017.....	74

CHAPTER 1. INTRODUCTION AND OBJECTIVES OF RESEARCH

1.1 Motivation for Study

Irrigation is the primary use of fresh water sources in the world (Kassam et al. 2007). Since fresh water resources are limited, it is essential to improve the efficiency of water use for agriculture, which can be achievable by managing irrigation optimally and reducing losses. Optimal irrigation management may include precise irrigation scheduling and an advanced level of management at the sub-field scale. Uniform irrigation include a uniform application of water across an entire field, which may lead to areas of under and over irrigation (Higgins et al. 2016). This is because there may exist variability in soil properties, topography, plant health, and pest pressure across the same field. Precise management of irrigation is limited using uniform application of water and hence, is a factor that restrains improvements in water use efficiency under these variable conditions. Sadler et al. (2005) emphasize the need to adopt more efficient irrigation systems for conservation of water in context of drought events, regulations on water use in various sectors, and water scarcity. Therefore, site-specific management of irrigation at a sub-field scale may prove beneficial for improving water use efficiency in agriculture.

Enhanced communication systems, improved sensing technologies, and capable control systems collectively allow the management of water application at a sub-field scale in center pivot sprinkler systems and lateral move irrigation systems (Kranz et al. 2012). With the evolution of site-specific irrigation or variable rate irrigation (VRI), it is possible to apply spatially varying amounts of water to the field with the potential of avoiding zones of excess and deficit water applications (Higgins et al. 2016). Various field studies and simulations presented the benefits from adoption of VRI (Lo et al. 2016;

O'Shaughnessy et al. 2016; Miller et al. 2017; Sui and Yan 2017). For example, Sadler et al. (2005) simulated site-specific irrigation in various case studies and estimated about a 10-15% reduction in water withdrawals over uniform irrigation method. They also discussed benefits other than reduced water withdrawals, such as reduced leaching, lower disease occurrences, and more harvestable area. West and Kovacs (2017) proposed the use of site-specific VRI using an unmanned aerial system and soil moisture sensors to encourage sustainable use of water resources and help reduce ground water withdrawals. Therefore, this section will discuss VRI as a potential tool to increase water efficiency in agriculture.

1.2 Literature Review

1.2.1 VRI Management Factors

Examining variability in different characteristics of a field is crucial to VRI management. Pan et al. (2014) addressed the importance of studying temporal changes in soil conditions for making accurate decisions on various agricultural inputs. They considered various factors, including soil apparent electrical conductivity and field elevation, while selecting locations for installation of soil moisture sensors to study heterogeneity in the field. Sadler et al., (2002) found statistically significant variation in crop response to irrigation in a field. They applied different irrigation treatments to study the variability in crop response to site-specific irrigation. Four irrigation treatments and two nitrogen treatments were applied to randomly arranged plots in a center pivot equipped field with highly variable soils. They found significant differences in yield due to varying irrigation application both among and within soil types. They recommended

division of the field into small management zones with similar soils and field characteristics to manage irrigation optimally, which may increase profitability. VRI may be implemented to mine undepleted soil water from areas of large soil water holding capacity in a field to reduce pumpage requirements for irrigation (Lo et al. 2016). On the other hand, Bramley and Hamilton (2005) studied spatial variability in winegrape yield in a vineyard situated in the Coonawarra region, South Australia. They found that winegrape yield within the study field varied an order of magnitude. They did not study the factors contributing to yield variability over study years, but suggested a shift from uniform management of the vineyard to zonal management.

An important factor contributing to spatial variation in crop yields across a field is variability in soil water content within a field. Kaleita et al. (2007) studied spatial variability and temporal stability in soil water content patterns in a field at a University of Illinois research farm in Urbana, Illinois. Soil water content patterns were correlated with topography of the field. Results indicated that temporal stability in water content patterns existed for over half of the field, and for the remaining half of the field, no temporal stability in water content patterns was observed. Furthermore, no major correlations were obtained between topographic features and soil water content patterns. A ten-meter scale was recommended for future soil water content sampling studies based on the results obtained from the study.

Evapotranspiration (*ET*) is a critical component of a soil water balance, which helps to determine irrigation requirements. Since *ET* can vary spatially within a field planted with same crop, it is vital to determine spatial *ET* when determining spatial plant

water requirements. Barker et al. (2018a) used a hybrid *ET* model (Neale et al., 2012) for managing VRI at two research sites in Nebraska. This model computes spatial *ET* across the field using remote sensing imagery. Howes et al. (2015) conducted a study on 15 center pivots located in Los Angeles County, near Palmdale, California. They used Landsat 5 satellite images processed with Mapping Evapotranspiration at High Resolution with Internal Calibration (METRIC) to map spatial *ET*. They found that there is a considerable effect of distribution uniformity of irrigation systems on the spatial variability of evapotranspiration in a field, especially during water stressed conditions. Their study reported that 55% of non-uniformity in spatial *ET* was caused by distribution uniformity of the irrigation system under crop water stressed conditions.

1.2.2 Remote Sensing in VRI

Recently, remote sensing has been used to map spatial variability in *ET* within a field. For example, Howes et al. (2015) utilized remote sensing images to examine spatial variability in *ET*. A common method of estimating spatial *ET* is the utilization of crop coefficients (K_c) based on remotely sensed vegetation indices (Barker et al., 2018b). Crop coefficients based on remotely sensed vegetation indices could be effectively utilized for estimation of spatial *ET* (Bausch and Neale 1987) and hence, this methodology could be used to manage VRI with different management zones (Stone, Bauer, and Sigua 2016). Bausch and Neale (1987) studied the correlation between a vegetative index and basal crop coefficient (K_{cb}) at the Northern Colorado Research and Demonstration Center near Greeley, CO. They estimated K_c by correlating them with the Normalized Difference Vegetative Index (NDVI). Neale et al. (2012) applied a hybrid approach to estimate *ET*

over cotton fields located at the USDA-ARS, Conservation and Production Research Laboratory (CPRL), in Bushland, TX. Another approach to estimate ET is by using an energy balance model, which considers radiative surface temperature of canopy. The hybrid approach is comprised of two components namely, the Two Source Energy Balance (TSEB; (Norman, Kustas, and Humes 1995) model and remote sensing-based K_c approach. In the hybrid model, TSEB model provided estimates of crop ET on the days when there were remote sensing inputs. For estimation of crop ET between days of remote sensing inputs, the reflectance-based K_c approach was used to compute crop ET . Hybrid model ET output was compared with ET measurements from eddy covariance systems to evaluate the performance of the hybrid approach. They found the hybrid approach performed reliably, improved the estimates of crop ET , and resulted in accurate soil water content estimation with the inclusion of ET from the TSEB model. The hybrid spatial ET model could also be effectively used for real time site-specific irrigation management (Barker et al., 2018b). They compared remote-sensing-based crop coefficient modeled ET , and TSEB computed ET with eddy covariance data to study model performance with different methodologies.

On a larger scale, Kukal et al. (2017) studied trends in ET spatially and temporally over the Great Plains region of the United States. Multiplatform satellite imagery was used to analyze ET over the period of 1982-2013. In conclusion, they found that satellite-based K_c could be adopted to estimate crop development and plant water use. Diarra et al. (2017) compared and evaluated the TSEB model and the FAO Irrigation and Drainage Paper No. 24 dual K_c approach for computing ET and evaluate the model performance. This study was conducted on four plots of wheat and sugar beet in the Haouz plain of

Marrakech, Morocco. The TSEB model in their study performed proficiently in comparison to the dual K_c approach to estimate ET on a large scale. The conclusion drawn from the study was that the TSEB model can be used to calculate actual ET and may help in creating irrigation scheduling decisions. Accurate estimation of spatial ET is crucial to design accurate VRI prescription maps.

1.2.3 VRI Management Systems

Though VRI allows more flexibility and control over irrigation management, it is complex and difficult to manage. Site-specific irrigation requires an expert system which can accurately study variability in soils and prescribe irrigation to reduce water withdrawals over uniform irrigation methods (Stone et al. 2015). O'Shaughnessy et al. (2016) used a comprehensive supervisory control and data acquisition (SCADA) system to estimate the potential benefits using VRI.

Additionally, center pivot VRI can be implemented in two ways, namely speed control and zone control. In speed control, the field is divided into small angular sectors based on spatial variability in the field. Zone control provides more control by allowing division of field into irregularly shaped management areas. These areas can then be precisely managed according to spatial characteristics of the field. Zone control VRI systems are more costly and complex than speed control VRI systems. The current use of zone control VRI is mainly to avoid irrigation on non-cropped areas of a field such as streams, waterways, ponds, roads, drainage ways, or rocky outcrops (Evans et al. 2013). This implies the need for studying and presenting other potential benefits from VRI, which could increase water use efficiency in irrigation sector.

In the past, a number of studies have reported application efficiencies of VRI-equipped center pivots. For example, Higgins et al. (2016) studied the application efficiency of a VRI system by two-dimensional layout of catch cans for measuring net irrigation applied through a center pivot system. About a 7% difference in water depth was observed between prescribed and measured depths. The largest differences were found in the areas where transitions occurred from one to another irrigation depth between management zones. They developed a criterion for designing minimum size of management zone for VRI management which was a function of characteristic length of transition from one zone to other zone. Yari et al. (2017) undertook a study to evaluate the performance of a VRI system versus a constant rate system on the basis of uniformity coefficients. The study was conducted on a five span center pivot sprinkler system at the Alberta Irrigation Technology Centre in southern Alberta, Canada during 2014 and 2015. While wind speeds were significant in reducing the application uniformity of the irrigation system, they reported that different application rates from the system did not affect the uniformity. Additionally, an updated sprinkler package on the pivot positively affected the uniformity coefficients and hence, it is important to have an appropriate knowledge of equipment such as age, wear and functionality. After computing different uniformity coefficients for both variable application and constant application experiments, they concluded that variable rate applications do not affect application uniformity of their center pivot irrigated system.

Various studies have been undertaken to evaluate VRI systems by comparing the yield and water response from VRI with a uniform irrigation, which is uniform irrigation managed by maintaining specific range of soil water deficit. Stone et al. (2015) managed

irrigation using four treatments on a field situated near Florence, South Carolina over the period of three years. The four treatments applied were VRI using an expert system for uniform irrigation in plots, VRI using an expert system to manage irrigation within plots according to individual soils, uniform irrigation based on maintaining specific soil water potential and a rainfed treatment. Results indicated that over the three-year study, the rainfed treatment had significantly lower yields than other three treatments. No significant differences in yields were observed among irrigated treatments. Additionally, they also found that water use efficiency was greater for the rainfed and uniform irrigation treatments than for both VRI treatments. They concluded that the expert system used in the study needed further improvement to manage VRI efficiently. Stone et al. (2016) conducted a similar study in which three irrigation treatments were compared: VRI using Irrigator Pro, uniform irrigated managed using remotely sensed K_c and uniform irrigation based on soil water potentials. No significant differences in yield and water use between VRI and uniform irrigation treatments were observed. They concluded that Irrigator Pro could be adequately implemented to manage irrigation. Barker et al. (2018a) undertook a field study to evaluate the performance of VRI compared to uniform irrigation and rainfed treatments. VRI was managed using two methods; VRI using a spatial ET model (Neale et al. 2012), and VRI using neutron probe soil water content. Other treatments were uniform irrigation and rainfed. They found that drift in their water balance model caused over application of water in the model-based VRI treatment. With current advancements in technologies such as improved computational capabilities and enhanced data management, development of VRI and evolution of plant and water

sensing technology, there is a potential to improve water use efficiency with the adoption of VRI.

1.2.4 Potential Benefits of Variable Rate Irrigation

Estimation of potential benefits of VRI has been studied in a number of studies by simulating VRI (Evans et al. 2013; Lo et al. 2016; Miller et al. 2017). O'Shaughnessy et al. (2016) presented the potential of increasing water use efficiency through the adoption of VRI using SCADA. Lo et al. (2016) quantified potential water withdrawal reductions from adopting VRI to account for variability in root zone AWC. The gridded Soil Survey Geographic database (gSSURGO; NRCS, 2014) was used to study variability in soils over the region and estimated that 51 mm per year water in 2% of the fields and 25 mm per year in 13% of the fields water withdrawals can be reduced with VRI. Adoption of zone control VRI in areas having large variability in soils and high pumping costs was recommended.

It is important to comprehensively quantify all benefits of VRI management to promote its adoption. Sadler et al. (2005) discussed the potential benefits from adoption of spatially varying irrigation in a field and concluded that future field research is needed to validate the concept of water and nutrient conservation through VRI. They added development of decision support and control systems for real-time monitoring could enhance the applications of precision irrigation or VRI. Extensive field testing is required to determine the economic feasibility and benefits of VRI to motivate producers to invest in this technology (O'Shaughnessy et al. 2016).

Adoption of VRI can also result in pumpage reductions by applying an optimal depth of water throughout a field (Sadler et al. 2005). Management of VRI using spatially varying soil available water capacity (*AWC*) may prove beneficial by producing optimal crop yield and water use efficiencies (Hedley and Yule 2009). Spatial *ET* along with spatial *AWC* will provide better estimates of spatial irrigation requirements for precise VRI management (Barker et al., 2018a). They suggested future research in the direction of VRI management in large commercial scale fields as well as economic analysis on the VRI system.

West and Kovacs (2017) studied the potential of managing VRI with remote sensing using an unmanned aerial system and soil moisture sensors to improve water use efficiency and reduce ground water pumpage and associated reduction in pumping costs. Further, they performed an economic analysis on soil moisture sensors and unmanned aerial systems for VRI management and reported that soil moisture sensors are more economical to adopt than unmanned aerial systems. They also added that cost of unmanned aerial systems has been decreasing, which may result in consideration of these systems as a potential and viable option for VRI management.

1.2.5 Conclusion

To conclude, irrigation systems need to be more efficient to meet future food requirements and use water resources sustainably. In uniform irrigation, irrigation is managed by treating the whole field as a homogeneous region. Since spatial variability may exist for various characteristics of a field such as soil types, slope, and soil water content, assuming field uniformity may lead to over or under watering certain areas

within the field. This restrains optimal irrigation management and further improvements in water use efficiency in irrigated systems. VRI is a technology that divides the field into small management zones based on spatial variability of the field. It may be considered as an option to improve water use efficiency, but there are many challenges that need to be overcome before VRI becomes beneficial and feasible for farmers to implement. An efficient decision control system needs to be developed, which is user friendly and is capable of creating precise real time prescriptions for VRI management. Additionally, zone-control VRI systems are expensive and additional research and development is needed to improve the economics for farmers, in most cases. VRI has potential for optimal management of irrigation, but there is a gap which needs to be filled before it could be adopted widely. This gap includes lack of comprehensive research, user-friendly accurate model for decision making in VRI, and economic viability for a broad range of applications.

1.3 Objectives

The research goal for the study was to evaluate a spatial *ET* model for VRI management in terms of crop yield improvement and water withdrawal reduction compared to uniform irrigation and rainfed methods at the production field scale. The uniqueness of the study as compared to past studies lies in terms of the scale of this study. This study is conducted at a quarter section field (53 ha), similar to commercial farms. This study is a continuation of the Barker et al. (2018a) study with improved methodology for old treatments and new treatment inclusions. We added several new components to the study including unmanned aerial system imagery for model input, soil

water measurements for reducing model drift, and an improved method of estimating deep percolation for improved estimation of water balance components. We hypothesized that VRI would result in reduced water withdrawal over other irrigation treatments, while minimizing yield reduction.

Following are the specific objectives:

1. Evaluation of VRI implemented using a spatial *ET* model by comparing crop yields and water withdrawals with uniform and rainfed treatments.
2. Continued development of a decision support system that simplifies the process of developing VRI prescription maps for easy management of VRI.
3. Address and examine the spatial variability in yields, soils and ET.

1.4 References

- Barker, J. B., Heeren, D. M., Neale, C. M. U., & Rudnick, D. R. (2018a). Evaluation of Variable Rate Irrigation Using a Remote-Sensing-Based Model. *Agricultural Water Management*, 203 63–74. doi:10.1016/j.agwat.2018.02.022
- Barker, J. B., Neale, C. M. U., Heeren, D. M., & Suyker, A. E. (2018b). Evaluation of a Hybrid Reflectance-Based Crop Coefficient and Energy Balance Evapotranspiration Model for Irrigation Management. *Transactions of the ASABE*, 61(2), 533–48
- Bausch, W. C., & Neale, C. M. U. (1987). Crop Coefficients Derived from Reflected Canopy Radiation : A Concept. *Transactions of the ASAE*, 30(3), 703–9
- Bramley, R. G. V., & Hamilton, R. P. (2005). Understanding Variability in Winegrape

- Production Systems 1. Within Vineyard Variation in Yield over Several Vintages. *Australian Journal Of Grape And Wine Research*, 10(1), 32–45. doi:10.1111/j.1755-0238.2004.tb00006.x
- Diarra, A., Jarlan, L., Er-raki, S., Page, M. Le, Aouade, G., Tavernier, A., Boulet, G., Ezzahar, J., Merlin, O., & Khabba, S. (2017). Performance of the Two-Source Energy Budget (TSEB) Model for the Monitoring of Evapotranspiration over Irrigated Annual Crops in North Africa. *Agricultural Water Management*, 193 71–88. doi:10.1016/j.agwat.2017.08.007
- Evans, R. G., LaRue, J., Stone, K. C., & King, B. A. (2013). Adoption of Site-Specific Variable Rate Sprinkler Irrigation Systems. *Irrigation Science*, 31(4), 871–87. doi:10.1007/s00271-012-0365-x
- Hedley, C. B., & Yule, I. J. (2009). A Method for Spatial Prediction of Daily Soil Water Status for Precise Irrigation Scheduling. *Agricultural Water Management*, 96(12), 1737–45. doi:10.1016/j.agwat.2009.07.009
- Higgins, C. W., Kelley, J., Barr, C., & Hillyer, C. (2016). Determining the Minimum Management Scale of a Commercial Variable-Rate Irrigation System. *Transactions of the ASABE*, 59(6), 1671–80. doi:10.13031/trans.59.11767
- Howes, D. J., Ellenson, S., Hoffmann, L., & Gaudi, F. (2015). Center Pivot Sprinkler Distribution Uniformity Impacts on the Spatial Variability of Evapotranspiration. *Journal of Irrigation and Drainage Engineering*, 141(8), 4014085. doi:http://dx.doi.org/10.1061/(ASCE)IR.1943-4774.0000851

- Kaleita, A. L., Hirschi, M. C., & Tian, L. F. (2007). Field-Scale Surface Soil Moisture Patterns and Their Relationship to Topographic Indices. *Transactions of the ASABE*, 50(2), 557–64
- Kassam, A. H., Molden, D., Fereres, E., & Doorenbos, J. (2007). Water Productivity : Science and Practice — Introduction. *Irrigation Science*, 25 185–88.
doi:10.1007/s00271-007-0068-x
- Kranz, W. L., Evans, R. G., Lamm, F. R., O’Shaughnessy, S. A., & Peters, R. T. (2012). A Review of Mechanical Move Sprinkler Irrigation Control and Automation Technologies. *Applied Engineering in Agriculture*, 28(3), 389–97
- Kukul, M., Irmak, S., & Kilic, A. (2017). Long-Term Spatial and Temporal Maize and Soybean Evapotranspiration Trends Derived from Ground-Based and Satellite-Based Datasets over the Great Plains. *Journal of Irrigation and Drainage Engineering*, 143(9), 1–18. doi:10.1061/(ASCE)IR.1943-4774.0001212.
- Lo, T., Heeren, D. M., Martin, D. L., & Mateos, L. (2016). Pumpage Reduction by Using Variable Rate Irrigation to Mine Undepleted Soil Water. *Transactions of the ASABE*, 59(5), 1285–98. doi:10.13031/trans.59.11773
- Miller, K. A., Luck, J. D., Heeren, D. M., Lo, T., Martin, D. L., & Barker, J. B. (2017). A Geospatial Variable Rate Irrigation Control Scenario Evaluation Methodology Based on Mining Root Zone Available Water Capacity. *Precision Agriculture*, 19(4), 666. doi:10.1007/s11119-017-9548-z
- Neale, C. M.U., Geli, H. M.E., Kustas, W. P., Alfieri, J. G., Gowda, P. H., Evett, S. R.,

- Prueger, J. H., et al. (2012). Soil Water Content Estimation Using a Remote Sensing Based Hybrid Evapotranspiration Modeling Approach. *Advances in Water Resources*, 50 152–61. doi:10.1016/j.advwatres.2012.10.008
- Norman, J. M., Kustas, W. P., & Humes, K. S. (1995). Source Approach for Estimating Soil and Vegetation Energy Fluxes in Observations of Directional Radiometric Surface Temperature. *Agricultural and Forest Meteorology*, 77(3–4), 263–93. doi:10.1016/0168-1923(95)02265-Y
- O’Shaughnessy, S. A., Evett, S. R., Andrade, M. A., Workneh, F., Price, J. A., & Rush, C. M. (2016). Site-Specific Variable-Rate Irrigation as a Means to Enhance Water Use Efficiency. *Transactions of the ASABE*, 59(1), 239–49. doi:10.13031/trans.59.11165
- Pan, L., Adamchuk, V. I., Ferguson, R. B., Dutilleul, P. R. L., & Prasher, S. O. (2014). Analysis of Water Stress Prediction Quality as Influenced by the Number and Placement of Temporal Soil-Water Monitoring Sites. *Journal of Water Resource and Protection*, 6 961–71. doi:http://dx.doi.org/10.4236/jwarp.2014.611091
- Sadler, E. J., Evans, R. G., Stone, K. C., & Camp, C. R. (2005). Opportunities for Conservation with Precision Irrigation. *Journal of Soil and Water Conservation*, 60(6), 371–78. <http://www.jswconline.org/content/60/6/371%5Cnhttp://www.jswconline.org/content/60/6/371.abstract?sid=cf2d2e56-fb1a-4b9f-9e28-b0082d69d3e7>

Soil Survey Staff. (2014). Web Soil Survey.

<http://websoilsurvey.sc.egov.usda.gov/App/HomePage.htm>

Stone, K. C., Bauer, P. J., Busscher, W. J., Millen, J. A., Evans, D. E., & Strickland, E. E. (2015). Variable-Rate Irrigation Management Using an Expert System in the Eastern Coastal Plain. *Irrigation Science*, 33(3), 167–75. doi:10.1007/s00271-014-0457-x

Stone, K. C., Bauer, P. J., & Sigua, G. C. (2016). Irrigation Management Using an Expert System, Soil Water Potentials, and Vegetative Indices for Spatial Applications. *Transactions of the ASABE*, 59(3), 941–48. doi:10.13031/trans.59.11550

Sui, R., & Yan, H. (2017). Field Study of Variable Rate Irrigation Management in Humid Climates. *Irrigation and Drainage*, 66(3), 327–39. doi:10.1002/ird.2111

West, G. H., & Kovacs, K. (2017). Addressing Groundwater Declines with Precision Agriculture: An Economic Comparison of Monitoring Methods for Variable-Rate Irrigation. *Water (Switzerland)*, 9(1),. doi:10.3390/w9010028

Yari, A., Madramootoo, C. A., Woods, S. A., & Adamchuk, V. I. (2017). Performance Evaluation of Constant Versus Variable Rate Irrigation. *Irrigation and Drainage*, 66(4), 501–9. doi:10.1002/ird.2131

CHAPTER 2. PERFORMANCE OF VARIABLE RATE IRRIGATION
MANAGEMENT USING A SPATIAL EVAPOTRANSPIRATION MODEL WITH
SATELLITE AND AIRBORNE IMAGERY UPDATED USING SOIL WATER
CONTENT MEASUREMENTS

Abstract

Variable Rate Irrigation (VRI) considers spatial variability in field and plant characteristics for irrigation management in agricultural fields. VRI may reduce water losses by applying optimum irrigation depth to all areas of field. This research aims to quantify the potential of VRI using a spatial evapotranspiration (*ET*) model in terms of relative crop and water response compared to a uniform and rainfed treatments. Irrigation treatments were (1) VRI using Landsat imagery (VRI-L), (2) VRI using unmanned aerial system (UAS) imagery (VRI-U), (3) uniform, and (4) rainfed treatments. These treatments were compared in a randomized experiment under maize and soybean production in a research field near Mead, Nebraska. An updated version of the Spatial Evapotranspiration Modeling Interface (SETMI; Geli and Neale, 2012) model was used to make prescriptions for VRI treatments. Imagery from Landsat and UAS coupled with soil water content measurements from neutron probe were used as inputs into the model. In 2017, we found that mean total gross prescribed irrigation depth (I_p) for VRI-L was not significantly different ($\alpha = 0.05$) than the I_p for the uniform treatment for maize. However, the I_p for the VRI-L treatment was significantly greater than the I_p for the uniform treatment for soybean. Differences in soybean yield were not found to be significant among treatments. Maize yield was significantly greater for uniform and VRI treatments than for the rainfed treatment. In 2018, I_p for soybean was highest for VRI-U

treatment followed by uniform, and VRI-L treatments. They all were significantly different from each other. No significant results in I_p for maize were observed. No differences in crop yield were found in 2018. In all crop-year combination, the VRI and uniform treatments had higher ET than the rainfed treatment.

2.1 Introduction

Irrigated agriculture constitutes the largest freshwater usage in United States with approximately 80% of freshwater used for agriculture (Schaible and Aillery, 2015). Agricultural production is becoming more intensified and more yield can be obtained per unit of land and water. Over the years, new efficient irrigation systems have been introduced with an objective of increasing water productivity (yield produced per unit of water diverted for irrigation) in agricultural fields. Center pivot irrigation systems equipped with sprinkler systems are one of the most efficient irrigation systems (O'Shaughnessy et al. 2016), constituting about 80% of total irrigated acreage in Nebraska (Johnson et al. 2011). Agricultural freshwater use in Nebraska is about 6.83 million acre-feet per year (Dieter et al., 2017).

Conventionally, irrigation is applied uniformly intending to apply an equal depth to all parts of the field. Uniform irrigation is often managed according to a soil in the field having low available water capacity (Daccache et al. 2015). Uniform irrigation may lead to various water losses, which may be in the form of runoff and deep percolation (DP). Production of high yields throughout a field with significant spatial variability in field characteristics may be difficult to achieve with uniform irrigation. Such variability may exist in terms of soil types, topography, pest attack, crop growth, and nutrient

availability (O'Shaughnessy et al. 2016). To account for spatial variability in water management, VRI can be implemented to manage irrigation with more control and precision. VRI systems can apply varying amounts of irrigation to different parts of a field during a single irrigation prescription (Hedley and Yule, 2009; Evans et al., 2013; Stone et al., 2016). This ability could be used to match irrigation prescriptions with spatially varying crop water needs. VRI can be speed control or zone control. The differences between the two options exist in terms of cost, control, and flexibility. Speed control VRI systems can vary irrigation depths only in angular sectors of a circle and cannot vary rates along the pivot lateral. Zone control VRI systems can apply varying amounts of water throughout a field by using the ability to control individual or banks of sprinklers along the pivot.

VRI management may consider variability in multiple field characteristics to generate irrigation prescriptions. VRI can account for both spatial and temporal variation in crop water needs. Lo et al. (2016) predicted that mining undepleted soil water from areas of large available water capacity (*AWC*) in a field can reduce pumpage for irrigation in Nebraska center pivot irrigated fields. Differences in *AWC* of a field were used to compute VRI prescriptions and potential reductions in energy and water withdrawals were estimated (Miller et al. 2017). Similar to these studies, this study also utilized the differences in *AWC* among different management zones to manage irrigation treatments.

Evapotranspiration is an important component of the soil water balance. Spatial *ET* estimates are useful to study for efficient management of VRI (Barker et al., 2018a). Spatial *ET* estimates help in computation of spatial plant water needs. Real time estimation and forecasting of spatial *ET* helps in computing real time dynamic VRI

prescription maps (Barker et al., 2018b). Studies have utilized water balance models based on remote sensing imagery to compute spatial *ET* (Barker et al., 2018a, Stone et al., 2015). Barker et al. (2018a) used a hybrid spatial *ET* model (Neale et al. 2012) to manage VRI on fields in Nebraska. The hybrid model included a water balance model based on reflectance-based crop coefficients (Neale, Bausch, and Heerman 1989) and the two-source energy balance model (TSEB; Norman et al., 1995). The reflectance-based crop coefficient model used vegetation indices to compute spatial crop coefficient (K_c); Spatial K_c was then used to compute spatial *ET*.

Improvements in software capabilities, center pivot VRI systems, communication advancements, and better sensing instruments have enabled irrigation to be managed with more control and flexibility. O'Shaughnessy et al. (2016) discussed the potential of supervisory control and data acquisition systems for VRI management. They discussed specific advantages of these enhanced decision support systems in their study. However, VRI is complex to manage and may be costly. Because of the complexity and undefined benefits, it is currently being used primarily for avoiding areas in fields like rock outcrops and streams or drainways (Evans et al. 2013). Future work is needed to document the benefits of VRI and economic viability of investing in VRI systems. Precise models are helpful to estimate water balance components and manage VRI efficiently and precisely.

A number of field studies on VRI have been conducted to quantify the benefits of VRI (Stone et al. 2015; Stone and Sadler 2016; Barker et al., 2018a ; Sui and Yan 2017). Significant crop yield increases or reduction in water withdrawals resulting from VRI adoption were not observed in most studies. Reduction in water withdrawals was

observed with VRI compared to uniform irrigation method in Sui & Yan (2017). Most studies are conducted at smaller scales, which may or may not be representative of commercial-field-scale agricultural production. Research is needed to evaluate the potential of VRI at commercial farm scale.

The overall objective of this study is to quantify potential benefits in terms of yield increases and reduction in water withdrawals with VRI management compared to uniform irrigation and rainfed treatments at a commercial producer sized field. A spatial *ET* model was fed with remote sensing inputs from satellite and UAS. Crop yield, prescribed gross irrigation depth, actual evapotranspiration (ET_a), and various irrigation efficiencies were compared among treatments. Specific objectives of the study included: (1) comparing different irrigation treatments in terms of crop yield and irrigation usage, (2) improving VRI management using spatial *ET* model and remote sensing inputs from different sources, and (3) comparing treatments using water balance response variables.

2.2 Material and Methods

2.2.1 Study Site

A field site equipped with a center pivot irrigation system was used to conduct the experiment in 2017 and 2018. The site was near Mead, Nebraska (41.165°N, 96.430°W) and is property of the University of Nebraska's Eastern Nebraska Research and Extension Center (ENREC). The field was irrigated with a Lindsay Corporation (Omaha, Nebraska) Zimmatic 8500 center pivot with Lindsay's Precision VRI system allowing individual sprinkler control. The field size was nearly 53 ha (Google Earth Pro, assessed on October 15, 2018).

The north and south halves of the field were planted with maize and soybean, respectively, in 2017 and rotated for each half in 2018. The VRI-equipped center pivot was installed in 2014. The center pivot consisted of 7 spans having a total lateral length of about 380 m with sprinklers fixed on top of the lateral pipe. Soils in the field were classified as silty clay loam and silt loam (gSSURGO, Soil Survey Staff, 2018). Crops were planted in straight rows running east-to-west. The tillage practice was no till and the field was covered with residue from previous seasons. A single crop was sown in each half every year, and cattle grazed the maize residue during winter. A uniform anhydrous ammonia injection applications were applied to the field in the autumn preceding maize planting next year close to planting.

2.2.2 Experimental Design

The maize and soybean crops were managed as two different fields. Plots were designed along crop rows. Similar to Barker et al. (2018a), the design of the study plots was a generalized randomized complete block design (RCBD). Treatments were randomly assigned to plots in each soil group and were randomized both years. The design included 108 plots: 72 plots in the north and 36 plots in the south (Figure 2.1). The plots were rectangular with length of ~ 61 m and width of ~ 37 m. Blocking was based on the range of *AWC* in each soil class. *AWC* of each plot was computed from estimated values of field capacity (*FC*) and at wilting point (*WP*) for each plot. Plots were grouped into six blocks for the north half and three blocks for the south half of the field. The number of blocks was dependent on the range of *AWC* values in each block. Each final

soil block had a similar range of *AWC* of soils. The maximum variability in *AWC* values for a 1.2 m soil profile in each block was less than 40 mm.

Four treatments in 2017: variable rate irrigation using SETMI and Landsat (VRI-L), uniform (based on neutron probe), uniform 2, and rainfed, were applied to plots in both the north and south halves of the field. There were twice as many uniform plots as other treatments. This is because a fourth intended treatment was omitted after the experiment began. The uniform treatment was applied to omitted treatment plots. The 108 plots were equally divided among the four treatments to form balanced design for both north and south halves of the field.

In 2018, a new treatment, VRI using SETMI and unmanned aerial systems imagery (VRI-U), was added to the study. In 2018, the north half had four treatments, VRI-L, VRI-U, uniform, and rainfed. The south half design had three treatments, excluding the VRI-L treatment. Only 54 plots in north half and 24 plots in south half were used in the 2018 analysis because a new treatment was dropped from the study. The design was balanced for south and unbalanced for north. In the north, more plots in each block were attributed to the new treatment (VRI-U) to gain more knowledge on these treatments.

Irrigation was managed according to computed plot-specific water balances for the plots in VRI treatments. For the uniform treatment, a single plot was chosen in each half of the field for irrigation management. These plots had *AWC* near the lower 10th percentile of *AWC* for plots under uniform treatment in the respective half of the field. Uniform 2 treatment in 2017 was also irrigated according to the water balance for the

selected plot in uniform treatment. Rainfed plots were not irrigated throughout the season.

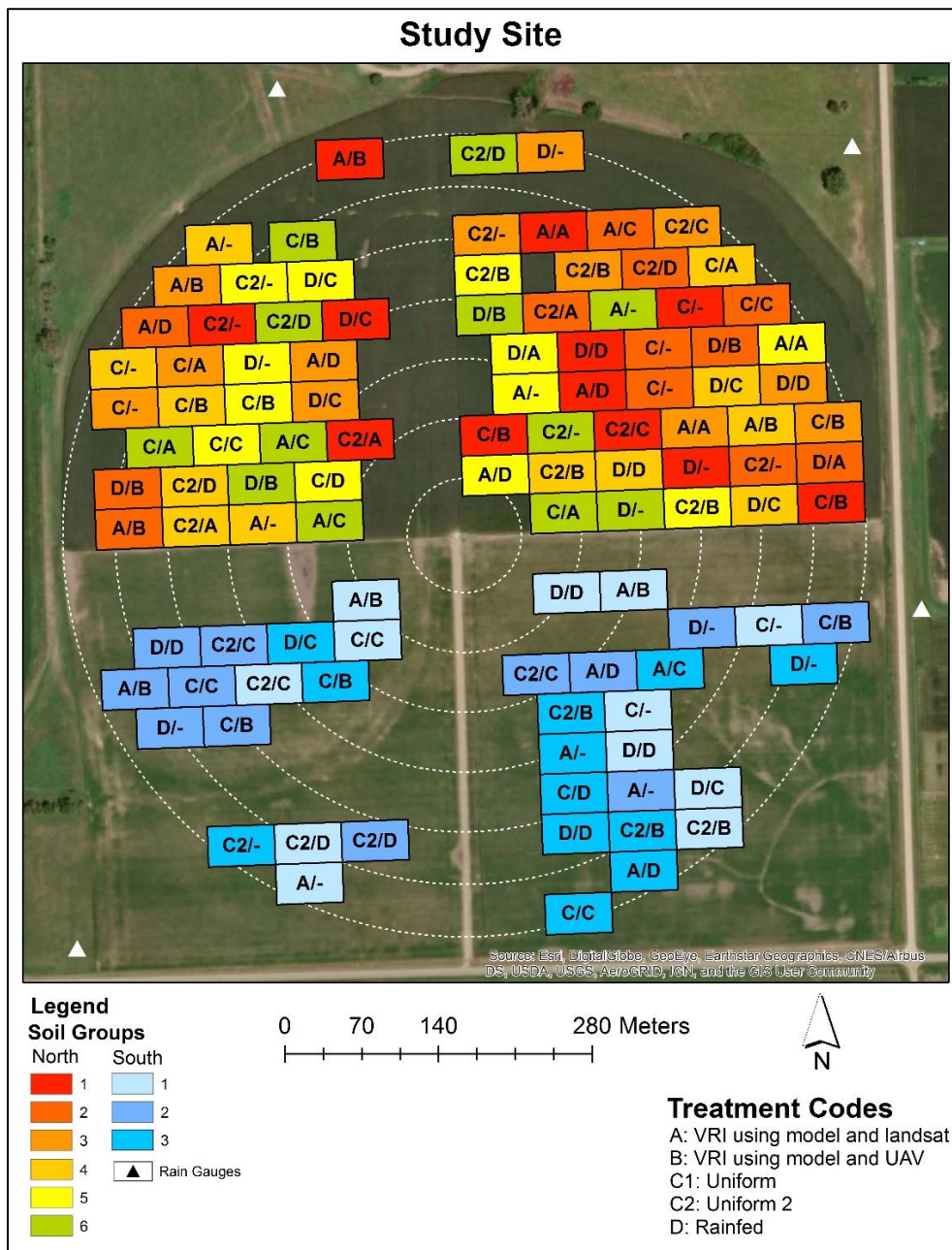


Figure 2.1 Plot layout of experiment in 2017 and 2018. Letters inside plots denote treatments applied in 2017/2018. Treatment are: A) VRI-L, B) VRI-U, C) Uniform, C2) Uniform 2, and D) Rainfed. '-' in plot labels is used to indicate that the plot was not used in the analysis for that year. Background basemap: World imagery from ESRI ArcMAP.

2.2.3 Acquired Data

2.2.3.1 Weather Data

Weather data was acquired from the High Plains Regional Climate Center's (HPRCC) data network called Automated Weather Data Network (AWDN). Data from The Memphis 5N (41.15°N, 96.417°W) weather station was used. This station was at a distance of approximately 1 km southeast of research field. Hourly and daily weather data from the station was used to compute reference evapotranspiration (ET_r) using the ASCE Standardized Tall Reference Evapotranspiration equation (ASCE-EWRI, 2005). ET_r was computed on hourly time step and summed up to daily step.

For irrigation scheduling, daily ET_r and growing degree days (GDD) were forecasted for remainder of the season after the most recent data. Daily average values of maximum and minimum air temperature (for GDD s) and ET_r were computed based on 20 years of historic weather data. Historic data from years 1997-2016 and 1998-2017 were used in 2017 and 2018, respectively. This data was obtained from the same weather station. These forecasted values along with forecasted K_c values were then used to predict crop evapotranspiration (ET_c). Finally, irrigation needs were computed using forecasted ET_c values.

Four tipping bucket type rain gauges were installed in different locations around the field. The rain gauges were Isco Model 764 (Teledyne Isco, Lincoln, NE) in 2017 and TR-525 USW (Texas Electronics) in 2018. Multiple rain gauges were used to accurately capture mean rainfall received by the field. Rain gauges were calibrated before installation. Correction values calculated in the calibration process were applied to the

data. The arithmetic mean of all four rain gauges was used to represent rainfall for a given day. Rainfall data was recorded on an event basis and the sum of events was used to represent rainfall on a daily basis. In 2018, rainfall data from weather station was used till 11 May due to erroneous measurements taken by field rain gauges due to improper installation.

Atmospheric pressure was obtained from Neb Field 3 Cosmic-ray Soil Moisture Observing System (COSMOS) station (Zreda, n.d.). Pressure data was used as an input into the TSEB model.

2.2.3.2 Remote sensing data

Remote sensing inputs from both satellite and UAS were used in the model. Satellite imagery from Landsat 7 Enhanced Thematic Mapper Plus (ETM+), Landsat 8 Operational Land Imager (OLI) and Landsat 8 Thermal Infrared Sensor (TIRS) were used in the model. The Level-1 raw and Level-2 surface reflectance imagery was retrieved from U.S. Geological Survey. Since Landsat 8 image becomes available after every 16 days, Landsat 7 imagery was used to increase the frequency of useful images. Images with cloud cover above the field or close were not used in the study. Some Landsat 7 images with missing data for the field were also not used. Therefore, these images were excluded from the study for that half. Atmospheric corrections for thermal infrared images were based on parameters calculated using Atmospheric Correction Parameter Calculator web application (Barsi, Barker, and Schott 2003). Ground-based pressure data and various weather parameters were used in obtaining parameters for atmospheric corrections. Thermal infrared images with low atmospheric transmission values (< 0.6)

were not used. Low transmissivity values indicate more error in temperature of images. Thermal infrared corrections were applied using ERDAS Imagine 2014 (Hexagon Geospatial, Madison, AL) software in 2017 and ArcGIS 10.4 (ESRI, Redlands, CA) in 2018.

In 2018, spectral imagery from UAS was collected using a MicaSense (Seattle, Washington) RedEdge multispectral sensor. The UAS imagery was captured at least once a week with exception with fewer imagery towards end of season due to logistical reasons. The imagery was taken at a ground resolution of approximately 17 cm. The imagery was processed and calibrated using Pix4D (San Francisco, California) software. It was scaled to resolution of 1 m to input into the model. ArcGIS (Esri, Redlands, California) software was used to scale and georeference the images.

2.2.3.3 Soil Water Content Data

Soil volumetric water content (θ) was monitored using neutron probe (NP) at the field. Two NPs, model 503 Elite Hydroprobe (CPN, Concord, California), were used to measure θ . Aluminum access tubes, having diameter of 5.1 cm, were used to monitor θ at different depths. The depths of measurement were 15, 30, 46, 76, 107, 137 and 168 cm for field. Tubes were installed near the geometric center of each plot. Tubes were installed between two plants with some offset distance from the crop row. Soil water content data was used to estimate soil water depletion within the root zone. θ measurements taken on a day were assumed to represent daily soil water status for end of that day. θ was monitored with a frequency of one to three weeks in 2017. Standard neutron counts were noted before and after the measurements were taken. Average

standard counts were used to convert soil neutron counts to θ . Thirty-second neutron count tests were used for θ measurement at a depth. The soil neutron count data obtained was then divided by average standard neutron count to obtain count ratio. Volumetric water content was obtained by using respective count ratios and probe's calibration slope and intercept coefficients.

Two NPs used in the study will be referred as probes E1 and E2, respectively. Both were locally calibrated using 22 soil samples from the field in 2017. The soil extracted during installation of tubes was used for soil sampling and site-specific calibration of NPs. The average length of soil samples used for calibration was about 10 cm with diameter of 4.1 cm. 60-second neutron counts were taken to be more accurate in calculations for calibration process. Each depth measurement of volumetric water content from probe was correlated to gravimetric water content obtained from oven drying method. The linear regression for the slope and intercept from the calibration were $0.3132 \text{ m}^3 \text{ m}^{-3}$ and $-0.1632 \text{ m}^3 \text{ m}^{-3}$, respectively for probe E1 and $0.2869 \text{ m}^3 \text{ m}^{-3}$ and $-0.1135 \text{ m}^3 \text{ m}^{-3}$, respectively for probe E2. The root mean square error (RMSE) in the calibration process was 0.018 for probe E1 and 0.019 for probe E2. Probes E1 and E2 needed firmware upgrades and maintenance after the 2017 season. Probe E1 needed new calibration coefficients in 2018 after probe was serviced. Probe E1 was cross-calibrated using probe E2. The new slope and intercept for probe E1 were $0.2766 \text{ m}^3 \text{ m}^{-3}$ and $-0.1189 \text{ m}^3 \text{ m}^{-3}$, respectively with $R^2 = 0.96$.

2.2.3.4 Soil sampling

Soil properties were determined for locations where access tubes were installed. *FC* and *WP* of each plot were estimated by Barker et al. (2018a). *FC* and *WP* were estimated for access tube location in each plot were assumed to represent *FC* and *WP* for the entire plot. *FC* was estimated using θ measurements from NP. *WP* was estimated using correlation with apparent electrical conductivity. *FC* values were updated in 2018 using neutron probe readings from 2017.

2.2.4 Water Balance Components

In modeling for the VRI-L, VRI-U, and uniform treatments, soil was assumed to be at *FC* before start of each growing season. This assumption was used due to off season recharge from precipitation at the field. Water balance calculations were computed with a daily time stamp and the end of the day happening at midnight. All measurements taken on a day were assumed to represent the end of that day. The root zone was grown linearly from a specified minimum to a maximum value (Barker et al., 2018a). The minimum value of the root zone depth used was 0.1 m and the maximum value was assumed to be 1 m for both crops. Initiation of root growth started at the emergence date computed as the day that basal crop coefficient (K_{cb}) first exceeded 0.12, and it was allowed to increase to its peak value when the K_{cb} reached their peak value. Projection of K_{cb} to its peak is discussed below.

2.2.4.1 Effective Rainfall

Rainfall data from the installed rain gauges at field site and the weather station were both used. Data from the rain gauges at field were used if data from both sources

were available. Rainfall data from the gauges at the field were more representative of rainfall received by the field. When recent data from these rain gauges were not downloaded, data from the weather station was used for irrigation scheduling purposes. The field rain gauge data were primarily used in the final analysis. The curve number method was used to compute runoff (SCS 1985). The curve number used for runoff calculations was 80. Runoff was subtracted from rainfall depth to get effective rainfall.

2.2.4.2 Evapotranspiration

For uniform irrigation plots, single K_c were employed to compute crop evapotranspiration (ET_c). Crop coefficients for maize were computed using mean K_c based on Allen & Wright, 2002. These coefficients were based on days after planting. For soybean, the average daily value of the two single K_c relationships (2007 and 2008) of Irmak, Odhiambo, Specht, & Djaman, (2013) was used. These coefficients were based on days after emergence. These coefficients were originally developed for Clay Center, Nebraska, which is approximately 160 km southwest of the field. The offseason single K_c was assumed to be 0.2. The day of year at which single K_c peaks out was estimated early in the season for irrigation forecasting. This estimation was done using 20-year historic daily average values of GDD and the previous season's GDD from planting to effective full cover.

For VRI treatments, dual crop coefficients were used in SETMI to compute ET . Reflectance based basal crop coefficients (K_{cbrf}) were computed based on the soil-adjusted vegetation index (SAVI) computed from remote sensing imagery. Using K_{cbrf}

relationships from Campos et al. 2017, ET_c was computed following FAO Irrigation and Drainage Paper No. 24 with equation:

$$ET_c = ET_r * K_c$$

where ET_c is crop ET , ET_r is alfalfa-based reference ET and K_c is crop coefficient. Dual K_c were used in the spatial ET model to compute ET for VRI treatments. Dual K_c were computed using following FAO Irrigation and Drainage Paper No. 24 with equation:

$$K_c = (K_{cb} * K_s) + K_e$$

where K_c is dual crop coefficient, K_{cb} is basal crop coefficient, K_s is water stress coefficient and K_e is soil evaporation coefficient.

2.2.4.3 Stored soil water

As mentioned in section 2.2.3.3, θ was monitored at 7 depths in the soil profile depth. Weighted average θ depth was used to represent stored θ in the water balance. Reading at 15 cm was assumed to represent 0 – 23 cm, 30 cm to represent 23 – 38 cm, 46 cm to represent 38 – 61 cm, 76 cm to represent 61 – 91 cm, 107 cm to represent 91 – 122 cm, 137 cm to represent 122 – 152 cm and 168 cm to represent 152 – 183 cm. However, a weighted average of θ down to a depth of 1 m, similar to modeled root zone depth, was used for water balance calculations.

2.2.4.4 Irrigation

Gross irrigation requirements were calculated from plot-specific water balances. A 9.1 m inner buffer zone inside the boundary of plots was used to allow time for

transitions between varying application depths (Barker et al., 2018a). The irrigation requirements were computed for the inner portion of the plot excluding the buffer area.

Manageable allowable depletion (*MAD*) was the threshold used for irrigation management. This was the soil water content threshold below which crop water stress was assumed to occur. The *MAD* used for maize was 50% of *AWC* before maturity was reached. Soybean was managed at 55% *MAD* until reproductive stage R2, after which *MAD* was reduced to 50% (Kranz, 2012). *MAD* was increased to 60% for both crops late in the season (Yonts, Melvin, and Eisenhower 2008). Soils were not irrigated to reach *FC*. Irrigating less than *FC* level allowed water to infiltrate into the soil from rainfall events. This rainfall allowance was chosen to be 25.4 mm. During real time irrigation management, irrigation requirements were forecasted every week. The maximum irrigation depth applied by the center pivot in a single pass was 30.48 mm. Irrigation depths were split into two or three prescriptions when irrigation requirements exceeded the maximum irrigation depth that could be applied by irrigation system in a single pass. Irrigation was applied to maintain root zone depletion less than *MAD* and greater than the rainfall buffer zone. This methodology is described by Barker et al. (2018a) and Barker et al. (2019).

The pivot typically took more than one day to complete a single irrigation event for one half of the field. For water balance calculations, the day when a plot received irrigation was computed based on average pivot travel time. If a plot received irrigation after midnight, it was considered to be irrigated on the next day similar to Barker et al., 2018a. Plots were considered irrigated if the pivot passed over the neutron access tube

location in the plot. The pivot was assumed to run at a constant speed, though speed varied in reality due to variable application depths. The speed was calculated using the start-stop time and angular distance covered.

Application efficiency was assumed to be 85% to account for losses such as evaporation, wind drift, etc. Gross irrigation was assumed to be the depth of water which was intended to be applied. Net irrigation was the assumed depth which infiltrated into the soil and could be utilized by plants. Net irrigation was computed after accounting for application efficiency in the gross irrigation.

Real-time adjustment of irrigation prescriptions due to rainfall was done if rainfall occurred after irrigation prescription development. If rainfall occurred before applying an irrigation prescription, the prescription was adjusted by reducing the rainfall amount from prescribed depth. In a case where rainfall happened during an irrigation event, the prescription was not adjusted for rainfall. In this case, the irrigation events were completed when it was feasible.

2.2.4.5 Deep percolation

Deep percolation was computed using different methods among the treatments. For the uniform and VRI-L treatments, instantaneous *DP* method was used which drained all water in excess of *FC* at end of the day (FAO Irrigation and Drainage Paper No. 24). This does not allow the depletion to go below 0 mm. A decaying function for *DP* (Raes et al., 2016) was used for the new VRI-U treatment in 2018 (Barker et al., 2019). Computation of *DP* for VRI-L and uniform treatments was done using instantaneous *DP* method only in 2018. This was done to stay consistent between methodologies for

treatments in 2017 and 2018. This allowed water in excess of FC to stay in the root zone to be used by plants for a few days. Also, depletion could go below 0 mm when using this method. This method was used during the final analysis.

2.2.5 SETMI Modeling for Irrigation Management

SETMI was embedded in ESRI's (Redlands, CA) geographic information system (GIS) software ArcGIS 10.4. SETMI (Geli and Neale 2012) was used to compute irrigation requirements for VRI-L and VRI-U plots. Dual K_c based on FAO Irrigation and Drainage Paper No. 24 were used in the model. Refer to Barker et al. (2018a) and Barker et al. (2019) for current information on SETMI in addition to the included water balance and TSEB models. Maize and soybean were considered as different fields in the model.

2.2.5.1 Water balance model

The offseason K_{cb} value was set to 0.12. K_{cbf} values were forecasted using two different methods depending on crop development (Barker et al., 2018b). The first method was used if the crop development was before full cover. This method projected the peak K_{cb} curve to day of the year at which K_{cbf} is expected to reach its peak value. Based on input imagery, a limit on how late this day could occur was estimated using last season's GDD to reach full cover from planting. At least two reflectance images were needed to project the K_{cb} curve to the peak value. The second method was followed after full cover. The day when the crop was expected to mature (reach an offseason SAVI value = 0.099) was input in SETMI. This input helps lower K_{cb} value at an appropriate rate after full cover. The end-of-season SAVI forecast was also used in final calculations for maize in 2017.

2.2.5.2 Two Source Energy Balance adjustment

Thermal infrared imagery was input into the TSEB (Norman, Kustas, and Humes 1995). The TSEB in SETMI can compute ET using different canopy latent heat flux equations (Barker et al., 2018b). The Priestly-Taylor equation was used to estimate canopy latent heat flux. As in Norman, Kustas, and Humes 1995, instantaneous ET which was calculated using TSEB model and scaled up to daily value (Barker et al., 2018b). The TSEB adjustment was not made for the VRI-U treatment, since the TSEB model was not extensively tested with UAS imagery as input. The TSEB was used to adjust ET and depletion (Neale et al. 2012) only for VRI-L treatment in both years.

TSEB ET was included in SETMI when the fraction of vegetation cover was above 20% for the majority of the field. Crop height and leaf area index, modeled based on Optimized Soil-Adjusted Vegetation Index values, were adjusted late in the season (Barker et al., 2018b). This adjustment was made to maintain crop height and leaf area index late in the season. Crop height and leaf area index images output from TSEB model at full effective cover (peak) were input into model late in the season to maintain peak values.

For VRI-L, TSEB ET was used to adjust the K_{cbrf} computed ET on each day a thermal image was input into SETMI. The adjustment was weighted based on a factor called Kalman gain or weighting factor (W) (Neale et al. 2012). Weighting factor can be changed from 0 to 1 to change the weight of TSEB ET in calculating the resulting ET after adjustment.

$$ET_{WB}^A = ET_{WB}^B + W(ET_{TSEB} - ET_{WB}^B) \quad (1)$$

where ET_{WB}^A , ET_{WB}^B are actual ET from water balance with and without adjustment using TSEB ET , respectively, and ET_{TSEB} is ET calculated by TSEB. We used weighting factor of 0.56 in computing actual ET .

TSEB ET could also update the soil water balance by adjusting the modeled depletion through the K_s . In case when the TSEB ET was lower than water balance ET , the K_s was decreased below unity. This would update the soil water balance by increasing depletion for the previous day. This new increased depletion for the previous day was then used to compute new depletion for the current day. However, in the case when TSEB ET was larger than water balance ET , the stress coefficient calculated in this case was 1, irrespective of a stressed condition that may be modeled by water balance.

2.2.5.3 Adjustment using measured soil water content

The output depletion from SETMI was adjusted using θ measurements from NP. Mean θ adjustment was used to adjust modeled depletion in 2017 and 2018. Four plots from the VRI-L and VRI-U treatments were selected for each of the two crop-year combination. These plots had θ values close to 0th, 33rd, 66th and 100th percentiles of the range of θ values on a measurement day among respective VRI-L and VRI-U plots. There were the most recent dates at which θ measurements were available at that time of selecting plots. Means of modeled depletion values from these four plots were compared to mean of measured values for the respective locations for each NP measurement date as:

$$\theta_{adj} = \theta_{mo} + (\overline{\theta_{ms}} - \overline{\theta_{mo}})$$

where θ_{adj} is the adjusted soil water content using measured soil water content from NP, θ_{mo} is modeled soil water content, $\overline{\theta_{ms}}$ is mean of measured soil water content for 4 plots and $\overline{\theta_{mo}}$ is mean of modeled soil water content for 4 plots. This adjustment was made on each measurement day in 2017 and 2018.

2.2.6 Data Analysis

The total prescribed gross irrigation depth was compared between treatments. Treatments were also compared using various response variables, including ET_a , crop yield, DP , change in soil water storage (ΔSW), irrigation water use efficiency ($IWUE$), evapotranspiration water use efficiency ($ETWUE$), and crop water use efficiency ($CWUE$). The various efficiencies were computed following Djaman & Irmak, 2012.

2.2.6.1 Computation of response variables

Seasonal water balances were modeled for each plot for computation of these variables. Similar to Barker et al. (2018a), analysis was performed between the first and last day of NP measurements. Unlike Barker et al. (2018a), SETMI was used to perform the final analysis. The measurement period in 2017 was from 18 April to 22 September for maize and from 9 May to 29 September. The measurement period in 2018 was from 23 April to 22 September for maize and from 8 May to 18-19 September for soybean. Last θ measurements for soybean in 2018 were taken in two days due to rainfall event happening later in the day on 18 September. Rainfall on 18 September was not included in water balance calculations for plots with last θ readings on 18 September since θ

readings were taken before the rainfall event for these plots. However, this rainfall event was included for plots with last θ readings on 19 September.

As discussed above that root zone depth of 1 m was used during irrigation management. During final analysis, depth of root zone was considered to be constant at 1.22 m for both crops. Weighted average of θ readings down to 1.22 m depth were used to represent soil water status on measurement dates. During final analysis, a decaying function (Raes et al., 2016; Barker et al., 2019) was used to simulate DP due to wetting events.

Landsat 7 and 8 imagery was used in SETMI for analysis in 2017. Due to sparse Landsat imagery in 2018, UAS imagery was used to run seasonal water balances and compute response variables in 2018. Peak SAVI values were based on imagery. For soybean, no end-of-season forecasted SAVI value was input late in the 2017 final analysis. Projected end SAVI value was input for maize due to lack of imagery close to end of season in both years. For soybean in 2018, projected end SAVI was also used. This input was used to end the K_{cbf} curve if there is no imagery close to maturity. The projected end SAVI was estimated based on visual observations of crop maturity close to end of season.

Soil evaporation was dampened by 25% for both crops to account for residue present in field. This adjustment was made following Barker et al. (2018a). Soil evaporation was also dampened during the season while computing water balance components. The amount of residue at field was estimated using the line transect method following (Shelton and Jasa 2009). Residue was estimated through multiple readings at

different locations in the field. The observations were taken at about 45° angle to crop rows.

2.2.6.2 Yield Processing

Crop yield was measured using yield monitoring equipment on harvesters. Yield data was filtered and cleaned using Yield Editor software version 2.0 (Agricultural Research Service, United States Department of Agriculture). These filters included moisture delay, maximum and minimum velocity, minimum swath, smooth velocity, maximum and minimum yield, standard deviation, overlap, and moisture adjustments. The filtered clean data was checked using mean yield (weight per unit area) reported for weighing grain carts. Plots were excluded from analysis if processed plot yield data points were less than 20 for maize and less than 25 for soybean within yield plot buffer in 2017. Threshold for excluding plots from 2018 analysis was less than 30 yield data points for both crops in 2018.

The yield analysis was done on the computed dry mass of crop grain yield. Mass of the moisture (using yield monitor measured moisture) present in grains during harvest was removed from grain mass while executing calculations for yield analysis.

2.2.6.3 Statistical Analysis

Similar to Barker et al. (2018a), multivariate analysis of variance (MANOVA) and univariate analysis of variance (ANOVA) were tests performed to study treatment and blocking effects of the response variables. SAS 9.4 (SAS Institute, Inc., Cary, NC) software was used to compute statistical analyses on the data. MONOVA tests and partial correlations between response variables was completed using PROC GLM. ANOVA

using PROC GLIMMIX was run and type III sum of squares and cross-products were calculated. Treatment differences were identified if each of these tests show significant results. Blocking was considered to be a fixed effect when these tests were performed.

Analysis on applied seasonal irrigation and response variables was done separately. The least mean squares mean were tested at 5% significance level.

2.3 Results and Discussion

2.3.1 Soil Properties

FC and *WP* were used to characterize different soils in the field. *FC* and *WP* for plots were computed using depth-weighted averages of *FC* and *WP* values at a location. Soil property estimates of *FC* and *WP* were used as in Barker et al. (2018a). In their study, *WP* was related to apparent electrical conductivity of soil. *WP* estimates had an uncertainty more than ± 0.1 to $\pm 0.2 \text{ m}^3 \text{ m}^{-3}$. *FC* was estimated using θ measurements from two days. The range of *FC* values was from 0.37 to $0.43 \text{ m}^3 \text{ m}^{-3}$ for north half and 0.37 to $0.41 \text{ m}^3 \text{ m}^{-3}$ for south half. *WP* values ranged from 0.17 to $0.21 \text{ m}^3 \text{ m}^{-3}$ for north and 0.18 to $0.20 \text{ m}^3 \text{ m}^{-3}$ for south. As a result, *AWC* values ranged from 0.17 to $0.25 \text{ m}^3 \text{ m}^{-3}$ for the north and 0.17 to $0.24 \text{ m}^3 \text{ m}^{-3}$ for the south.

In 2018, *FC* values for plots were updated using θ measurements taken in 2017. Irrigation requirements for a selected plot in the uniform treatment were small for early in the 2018 growing season. Consequently, there was less confidence in *FC* numbers from Barker et al. (2018a). θ readings from June 19, 2017 and May 12, 2017 were used to update *FC* numbers for plots in the north and south halves of the field, respectively. New *FC* values for the north plots ranged from 0.37 to $0.45 \text{ m}^3 \text{ m}^{-3}$. The *FC* range was 0.38 to

0.44 m³ m⁻³ for the south plots. The new *FC* numbers, in general, were greater than the values used in 2017. This resulted in an increase in *AWC* for most of the plots.

2.3.2 Rainfall

Historic (1981-2010) average rainfall from May to October was about 540 mm near the research field (NCEI, n.d.-a). This data was recorded by National Climatic Data Network's weather station Mead 6S which was situated about 6.5 km southwest of the field. The cumulative rainfall for months May to October recorded by the rain gauges at the field was 691 mm in both 2017 and 2018. These two years could be considered wetter than normal years.

2.3.3 Remote Sensing Imagery

Satellite imagery was used as a remote sensing input in 2017. Both Landsat 7 and 8 imagery were used in the model. Images with cloud cover were excluded from the model. Few Landsat 7 images were usable for the field (Table 2.1). Only one Landsat 7 imagery each for the north and south halves of the field was considered good.

Spectral UAS imagery was used in 2018 for the VRI-U treatment. Table 2.2 is a list of imagery used for irrigation scheduling and end-of-season analysis.

Table 2.1 List of dates of satellite imagery used in VRI-L treatment in 2017 and 2018.

Image Dates in 2017			Image Dates in 2018		
Satellite	Date	TSEB	Satellite	Date	TSEB
<i>Maize 2017</i>			<i>Soybean 2018</i>		
Landsat 8	May 13, 2017	No	Landsat 7	May 8, 2018	No
Landsat 8	May 29, 2017	No	Landsat 8	May 16, 2018	No
Landsat 7	June 6, 2017	No	Landsat 7	May 24, 2018	No
Landsat 8	June 14, 2017	Yes	Landsat 8	June 1, 2018	No
Landsat 8	June 30, 2017	Yes	Landsat 8	July 3, 2018	Yes
Landsat 8	July 16, 2017	Yes	Landsat 7	July 11, 2018	No
Landsat 8	August 17, 2017	Yes	Landsat 8	July 19, 2018	Yes
Landsat 8	September 2, 2017	Yes			
<i>Soybean 2017</i>					
Landsat 8	May 29, 2017	No			
Landsat 8	June 14, 2017	No			
Landsat 8	June 30, 2017	Yes			
Landsat 8	July 16, 2017	Yes			
Landsat 8	August 17, 2017	Yes			
Landsat 7	August 25, 2017	No			
Landsat 8	September 2, 2017	Yes			
Landsat 8	October 20, 2017	No			

Table 2.2. List of UAS images used in 2018.

No. of images	Date
<i>Maize & Soybean 2018</i>	
1	May 10, 2018
2	May 30, 2018
3	June 5, 2018
4	June 18, 2018
5	June 27, 2018
6	July 2, 2018
7	July 6, 2018
8	July 11, 2018
9	July 24, 2018
10	August 1, 2018
11	August 9, 2018
12	August 29, 2018
13	September 17, 2018
14	September 26, 2018

2.3.4 Eliminated Data

In 2017, two plots (16 and 2) were not used in the analyses for maize, the plots were part of VRI-L and rainfed treatments, respectively. The eliminated plot in VRI-L had an accidental spill of water on the neutron access tube which may result in erroneous soil water status in that plot. This plot was also used to correct the model using θ measurements. The spill of water occurred after irrigation prescriptions were applied in 2017. The other excluded plot in rainfed was due to low yield data points. No plot was excluded for soybeans.

In 2018, five plots in soybean and one plot in maize were excluded from final analysis due to less yield data points for these plots. In soybean, excluded were one plot from VRI-L, VRI-U, and rainfed each and two plots from uniform. In maize, excluded plot was from the uniform treatment.

2.3.5 Mean Total Gross Prescribed Irrigation Depth

In this section, treatment differences for I_p applied to the crop during a growing season are discussed. The rainfed treatment plots received no irrigation throughout the season. In 2017, total gross prescribed irrigation depth (I_t) for plots under VRI-L treatment ranged from 56 to 107 mm (Figure 2.1). Plots under uniform and uniform 2 treatments received equal I_p (Table 2.3). For maize, I_p was 77 mm for VRI-L treatment and 76 mm for the uniform and uniform 2 treatments. Treatment differences were not found to be significant. Contrary to these results, Barker et al. (2018a) found that I_p applied for VRI-L treatment was significantly greater than the uniform treatment in maize for this site during their two-year field study in 2015 and 2016. Rainfall during the

growing season of 2015 and 2016 was also greater than normal years. Their study did not include θ measurements in the model. We observed that model adjustments using measured soil water content decreased the irrigation requirements prescribed by the model. For soybean, I_p for the uniform and uniform 2 treatments (51 mm) was significantly lower than I_p for the VRI-L (76 mm) treatment. The range of I_t was 56 to 87 mm for the VRI-L treatment. Lower irrigation needs for the uniform treatment could be attributed to management using a plot that needed relatively less amount of water.

In 2018 for maize crop, I_p for VRI-U (64 mm) and uniform (66 mm) treatments were not different from each other. For soybean, I_p was 98 mm for VRI-U, 91 mm for uniform, and 70 mm for VRI-L. Significant differences in soybean were observed between all treatments. Less water was prescribed to the VRI-L treatment signifying a considerable reduction in water withdrawals over the uniform and VRI-U treatments. A

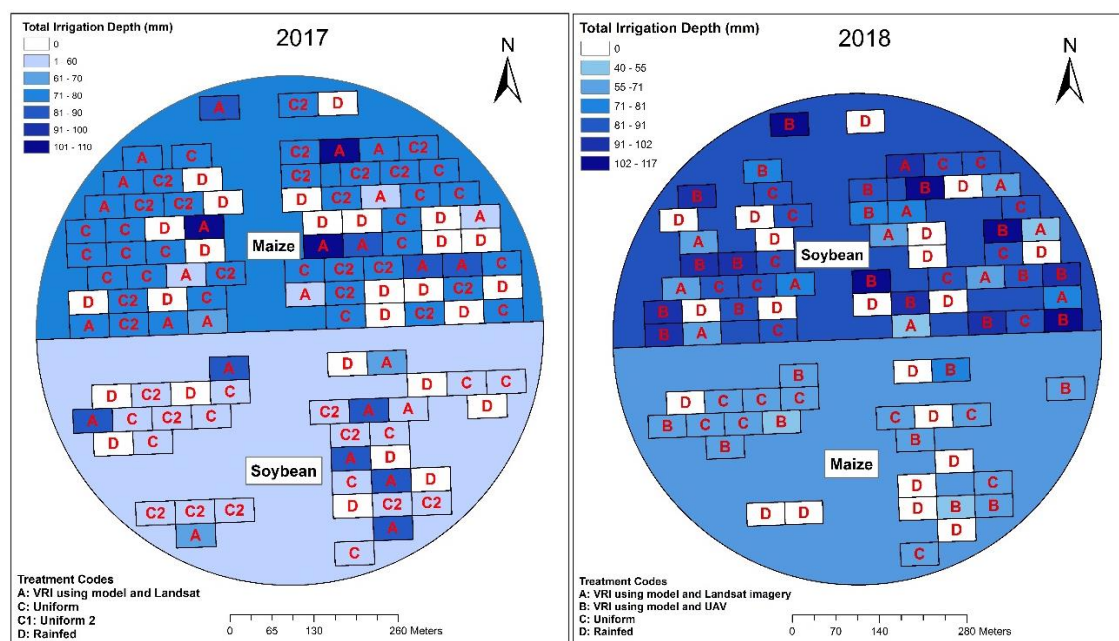


Figure 2.2 Total mean prescribed irrigation depth for each plot in 2017 and 2018.

Table 2.3. Mean total seasonal gross irrigation prescribed for treatments in 2017 and 2018.

2017			2018		
Treatment	Mean \pm SE (mm)	DF	Treatment	Mean \pm SE (mm)	DF
<i>Maize</i>			<i>Maize</i>		
VRI-L	76.5 \pm 3.3	12	VRI-U	63.8 \pm 1.9	22
Uniform	76.2		Uniform	66.0	
Uniform 2	76.2		Rainfed	0	
Rainfed	0				
<i>Soybeans</i>			<i>Soybeans</i>		
VRI-L	76.2 \pm 4.4	6	VRI-L	70.3 \pm 2.8	40
Uniform	50.8		VRI-U	97.6 \pm 2.3	40
Uniform 2	50.8		Uniform	91.4	
Rainfed	0		Rainfed	0	

small difference in I_p was observed between the VRI-U and uniform treatments. We acknowledge this difference to be small and non-practicable.

2.3.6 Correlation Among Response Variables

Table 2.4. Partial correlation coefficients for response variables.

Maize 2017					Maize 2018				
DF = 61	ET_a	DP	ΔSW	Yield	DF = 29	ET_a	DP	ΔSW	Yield
	1	-0.59	-0.75	0.37		1	-0.84	-0.69	-0.55
		1	0.05	-0.31			1	0.24	0.2
			1	-0.16				1	0.77
				1					1
Soybean 2017					Soybean 2018				
DF = 30	ET_a	DP	ΔSW	Yield		ET_a	DP	ΔSW	Yield
	1	-0.1	-0.83	-0.19		1	-0.93	0.09	0.14
		1	-0.43	-0.21			1	0.03	-0.06
			1	0.37				1	0.22
				1					1

As in Barker et al. (2018a), calculations were performed to test correlations between various response variables. The correlations were tested at a significance level of 10%. Table 2.4. is a summary of all correlations matrices. In 2017, we found significant correlation between ΔSW and ET_a for both crops ($P < 0.0001$). Other significant correlations included ET_a with yield ($P = 0.003$), ET_a with DP ($P < 0.0001$), and yield with DP ($P = 0.013$) for maize. Other significant correlations for soybean were between ΔSW and DP ($P = 0.016$), and ΔSW and yield ($P = 0.039$). In 2018, significant correlations for maize were observed between ET_a with DP ($P < 0.0001$), ΔSW and ET_a ($P < 0.0001$), ET_a with yield ($P = 0.002$), and ΔSW & yield ($P < 0.0001$). For soybean, only significant correlation was observed between DP and ET_a ($P < 0.0001$).

2.3.7 MANOVA and Univariate ANOVA Test Results

2.3.7.1 MANOVA test

Statistical analyses in this section were performed to test the hypothesis that there will be no significant differences in yield and ET_a between treatments. In the uniform treatment, irrigation was managed based on 90% irrigation adequacy (Lo et al. 2016) and hence, most parts of the field were sufficiently irrigated to prevent yield reduction. In years with normal rainfall amounts, fields dependent solely on rainfall produce good yields in proximity to the study site. It was expected that the rainfed treatment will perform well in years receiving normal rainfall. The results of the tests for the 2017 and 2018 data are discussed below.

MANOVA test were performed to determine overall treatment and blocking effects for all fields. Differences in response variables between treatments and soil blocks

were tested at a significance level of 5%. Wilks' lambda statistic was used to study these effects.

We found that treatments had a significant overall effect on response variables for both crops in 2017 and 2018 ($P < 0.0001$). Hence, data provided enough evidence to reject the null hypothesis that there were no treatment differences. The blocking effect was also significant for both crops in 2017 ($P < 0.0001$ for maize & $P = 0.0265$ for soybean in 2017). Univariate ANOVA tests were carried out after MANOVA results were found to be significant. In 2018, blocking effect was not significant for maize.

2.3.7.2 Univariate ANOVA tests

Individual univariate ANOVA tests for both crops were performed to study differences in response variables for all treatments. Results for four response variables: ET_a , DP , ΔSW , and yield, are discussed. All effects were tested at a 5% significance level. Overall, the treatment had a significant effect on ET_a for both crops in 2017 ($P = 0.0001$). We were able to reject the null hypothesis when ET_a was compared for these cases. Significant differences were also found in ΔSW and yield due to treatment effect for maize in 2017.

2.3.7.3 Least Squares Means of Response Variables

Table 2.5 is a summary of estimated least squares means from the ANOVAs for various response variables in each treatment for all crop year combinations (see also Figure 2.2). In 2017, the mean yield for different treatments in soybean ranged between 4 and 4.1 Mg ha⁻¹. Plot yield ranged from 3.4 to 4.4 Mg ha⁻¹. Significant differences in

Table 2.5. ANOVA test results for different response variables with least squares mean and multiple ranges groupings

Treatment	ET_a (mm)	DP (mm)	ΔSW (mm)	Yield (Mg ha ⁻¹)
	M ± SE	M ± SE	M ± SE	M ± SE
<i>Maize 2017</i>				
VRI-L	552 ± 5.7 a	52.3 ± 3.1 a	-21 ± 4.5 a	12.2 ± 0.2 a
Uniform	557 ± 5.5 a	53.1 ± 3.0 a	-26.4 ± 4.3 a	12 ± 0.2 ab
Uniform 2	557 ± 5.5 a	49.9 ± 3.0 a	-23.1 ± 4.3 a	12.3 ± 0.2 a
Rainfed	496 ± 5.7 b	50.5 ± 3.1 a	-39.3 ± 4.5 b	11.6 ± 0.2 b
<i>Soybean 2017</i>				
VRI-L	545 ± 9.2 a	105 ± 4.9 a	-67.3 ± 9.9 a	4.0 ± 0.1 a
Uniform	511 ± 9.2 b	106 ± 4.9 a	-59.3 ± 9.9 a	4.1 ± 0.1 a
Uniform 2	523 ± 9.2 ab	102 ± 4.9 a	-66.8 ± 9.9 a	4.0 ± 0.1 a
Rainfed	477 ± 9.2 c	111 ± 4.9 a	-81.5 ± 9.9 a	4.1 ± 0.1 a
<i>Maize 2018</i>				
VRI-U	597 ± 9.3 a	40.4 ± 6.5 a	-11.7 ± 5.1 a	12 ± 0.18 a
Uniform	595 ± 9.9 a	45.2 ± 6.8 a	-12.7 ± 5.4 a	12.2 ± 0.19 a
Rainfed	531 ± 9.3 b	39.6 ± 6.5 a	-8.5 ± 5.1 a	12.1 ± 0.18 a
<i>Soybean 2018</i>				
VRI-L	550 ± 9.7 a	43.6 ± 8.3 a	-37.6 ± 5.9 a	3.4 ± 0.08 a
VRI-U	567 ± 7.8 a	54.5 ± 6.7 a	-38.8 ± 4.7 a	3.4 ± 0.06 a
Uniform	565 ± 10.4 a	48.9 ± 8.9 a	-43.2 ± 6.3 ab	3.3 ± 0.08 a
Rainfed	505 ± 9.7 b	19.6 ± 8.4 b	-57.4 ± 5.9 b	3.4 ± 0.08 a

soybean yield were not found among treatments. This may be a result of having adequate water availability from rainfall for soybean. Thus, more water in irrigated plots did not increase the yield for soybean in 2017. For maize, mean yield ranged from 11.6 to 12.3 Mg ha⁻¹. Minimum and maximum plot yield was 8.3 and 13.4 Mg ha⁻¹ respectively. The minimum yield was found in one of the rainfed plots. Significantly greater maize yield was observed for VRI-L (12.2 Mg ha⁻¹) and uniform 2 (12.3 Mg ha⁻¹) treatments than for the rainfed (11.6 Mg ha⁻¹) treatment. We may attribute increased yields as compared to

rainfed plots to be due to irrigation applied to the VRI-L and uniform 2 treatments. Mean yield for the uniform (12 Mg ha⁻¹) treatment was greater than the rainfed (11.6 Mg ha⁻¹), but it was not significantly different. Results were observed that irrigation improved maize yield over rainfed treatment in 2 out of 3 cases.

No significant differences in maize yield were observed in 2018. All treatments performed similar to each other. The mean yield of the VRI-U treatment was 12 Mg ha⁻¹. Converse to results observed in 2017, the rainfed treatment performed similar to irrigated treatments. This could be attributed to better distribution of rainfall events during the vegetative stages of maize in 2018. Mean yield for the rainfed treatment observed was 12.1 Mg ha⁻¹. Rainfall in 2018 may have been adequate to keep crop free from significant water stress and to produce adequate yield when compared to other irrigated treatments.

As discussed above, there were treatment differences found in mean seasonal ET_a for both crops. In 2017, the rainfed (496 mm) treatment had significantly lower ET over

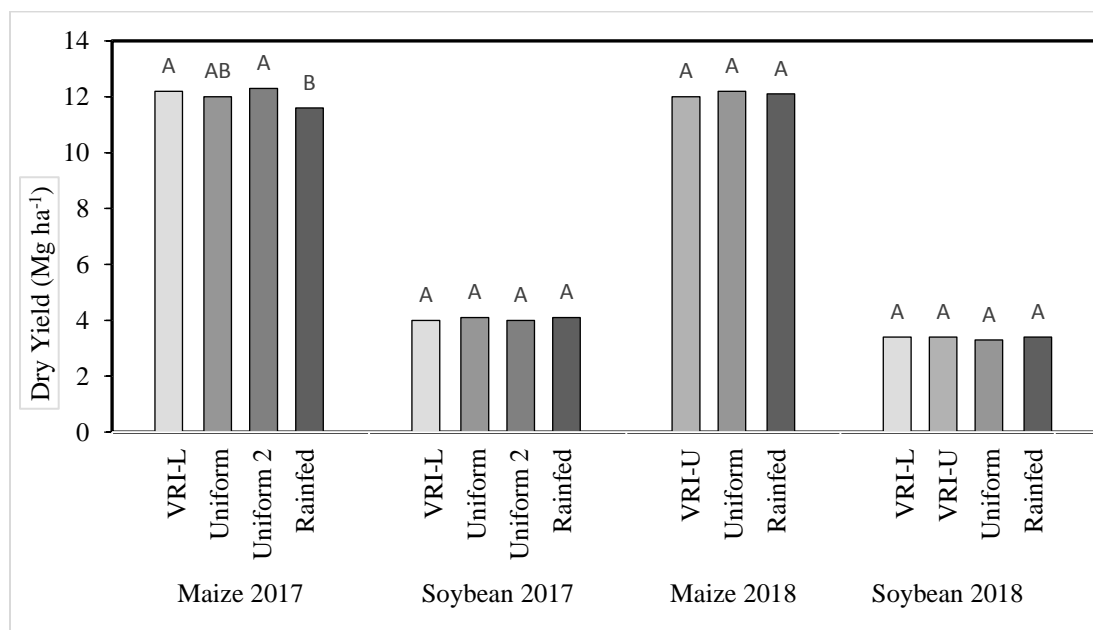


Figure 2.3. Dry yield for treatments for maize and soybean in 2017.

other treatments for maize. Mean *ET* was largest for uniform and uniform 2 treatments with 557 mm for maize. As expected, *ET* was correlated with yield for maize crop. treatments as compared to the rainfed treatment did not result in higher yield. Greater *ET* calculations in the VRI-L and uniform treatments could be attributed to overestimation of *ET* through under estimation of *DP* and runoff.

In 2018, mean *ET* for maize was larger for irrigated treatments than rainfed treatment. This trend was not observed in maize yield. Mean *ET* was largest for VRI-L (597 mm), followed by the uniform treatment (595 mm). Rainfed (531 mm) had significantly lower mean *ET* than VRI-L and uniform. For soybean, Mean *ET* for VRI-U and uniform was significantly larger than rainfed and VRI-L. Mean *ET* was 565 mm for uniform and 567 mm for VRI-U. Rainfed had significantly lowest *ET* than other treatments. These *ET* differences did not also result in differences in yield among treatments.

Computed mean *DP* was only found significantly different for soybean in 2018. Mean *DP* was lowest for rainfed (19.6 mm) than other irrigated treatments. Among other irrigated treatments, VRI-L (43.6 mm) had lowest *DP* and VRI-U had highest *DP* (54.5 mm), but they were not significantly different from each other. Thus, we did not find any significant reduction in *DP* with VRI treatments in comparison to the uniform treatment. Mean ΔSW was different among treatments in case of maize in 2017 and soybean in 2018. For both cases, rainfed had lowest ΔSW compared to other treatments. This signify that less water was available in the root zone soil layer at the end of the season for rainfed in these cases.

Three efficiencies were computed to compare the performance of the irrigation treatments. The efficiencies computed for different treatments and crops are given in Table 2.6. In 2017, *IWUE* for maize varied from 6.6 kg ha⁻¹ mm⁻¹ for uniform to 9.3 kg ha⁻¹ mm⁻¹ for the uniform 2 treatment. Irrespective of the uniform and uniform-2 treatments being similar, *IWUE* was different for these two treatments suggesting more factors than just applied irrigation contributing to changes in water use efficiency. The VRI-L treatment achieved a *IWUE* of 8.4 kg ha⁻¹ mm⁻¹. *IWUE* for soybean ranged from -0.7 kg ha⁻¹ mm⁻¹ for uniform 2, and VRI-L treatments to 0.2 kg ha⁻¹ mm⁻¹ for the uniform treatment. Positive values for maize indicate increased yield with irrigation. Values for soybean indicate that there was no meaningful yield improvement with irrigation as expected from Table 2.5. In 2018, maize had *IWUE* ranging from 0.1 kg ha⁻¹ mm⁻¹ for the uniform treatment to -2 kg ha⁻¹ mm⁻¹ for the VRI-U treatment. For soybean, lowest *IWUE* was observed in uniform (-1.2 kg ha⁻¹ mm⁻¹). VRI-L had *IWUE* of 0.5 kg ha⁻¹ mm⁻¹ and VRI-U had *IWUE* of 0.6 kg ha⁻¹ mm⁻¹.

ETWUE was also computed in the study. In 2017, maize had *ETWUE* values of 11 kg ha⁻¹ mm⁻¹ for VRI-L, 11.4 kg ha⁻¹ mm⁻¹ for uniform 2 and 8 kg ha⁻¹ mm⁻¹ for uniform. For soybean, *ETWUE* values were -0.7 kg ha⁻¹ mm⁻¹ for VRI-L, -0.8 kg ha⁻¹ mm⁻¹ for uniform 2, and 0.4 kg ha⁻¹ mm⁻¹ for uniform. In 2018, the range of *ETWUE* for maize was from -1.9 kg ha⁻¹ mm⁻¹ for VRI-U and 0.1 kg ha⁻¹ mm⁻¹ for uniform. Range of values for soybean was -1.9 kg ha⁻¹ mm⁻¹ for uniform and 0.9 kg ha⁻¹ mm⁻¹ for VRI-U.

CWUE in 2017 ranged from 21.5 kg ha⁻¹ mm⁻¹ for the uniform treatment to 23.4 kg ha⁻¹ mm⁻¹ for the rainfed treatment for maize. It ranged from 7.3 kg ha⁻¹ mm⁻¹ for the

Table 2.6. Different water use efficiencies for treatments for maize and soybean in 2017 and 2018.

Treatment	<i>IWUE</i>	<i>ETWUE</i>	<i>CWUE</i>
	(kg ha ⁻¹ mm ⁻¹)	(kg ha ⁻¹ mm ⁻¹)	(kg ha ⁻¹ mm ⁻¹)
	M	M	M
<i>Maize 2017</i>			
VRI-L	8.4	11	22.1
Uniform	6.6	8	21.5
Uniform 2	9.3	11.4	22.1
Rainfed	-	-	23.4
<i>Soybean 2017</i>			
VRI-L	-0.7	-0.7	7.3
Uniform	0.2	0.4	8
Uniform 2	-0.7	-0.8	7.7
Rainfed	-	-	8.6
<i>Maize 2018</i>			
VRI-U	-2	-1.9	20
Uniform	0.1	0.1	20.4
Rainfed	-	-	22.6
<i>Soybean 2018</i>			
VRI-L	0.5	0.7	6.2
VRI-U	0.6	0.9	6
Uniform	-1.2	-1.9	5.8
Rainfed	-	-	6.7

VRI-L treatment to 8.6 kg ha⁻¹ mm⁻¹ for the rainfed treatment for soybean. Values for *CWUE* indicate that the rainfed treatment was most efficient in using *ET* to produce yield. In 2018, rainfed had the greatest *CWUE* among treatments with 22.6 kg ha⁻¹ mm⁻¹ for maize and 6.7 kg ha⁻¹ mm⁻¹ for soybean.

2.3.8 Modeling Differences using UAS and Landsat Imagery

2.3.8.1 Spatial Resolution of Both Systems

Landsat 7 and 8 capture images at a 30 m ground resolution for multispectral imagery (green, red, and near-infrared bands), and 100 m and 70 m resolution for thermal infrared imagery taken from Landsat 8 and 7, respectively (NASA website, assessed on 20 November, 2018). Modeling water balance components using these resolutions may not be sufficient to study spatial variability at a sub-field scale. This can be observed in Figure 2.3 (a) and 2.3 (b) where a Landsat thermal infrared imagery processed to 30 m resolution (USGS, 2018) is shown underlying the experimental plots. The color in the plots depicts the values of SAVI. Figure 2.3 (a) is an image of modeled SAVI for 5 experimental plots and lowest SAVI value observed was 0.57.

Figure 2.4 (a) and 2.4 (b) are images of SAVI values computed using UAS imagery for same set of plots as in Figures 2.3 (a) and 2.3 (b). The UAS thermal infrared

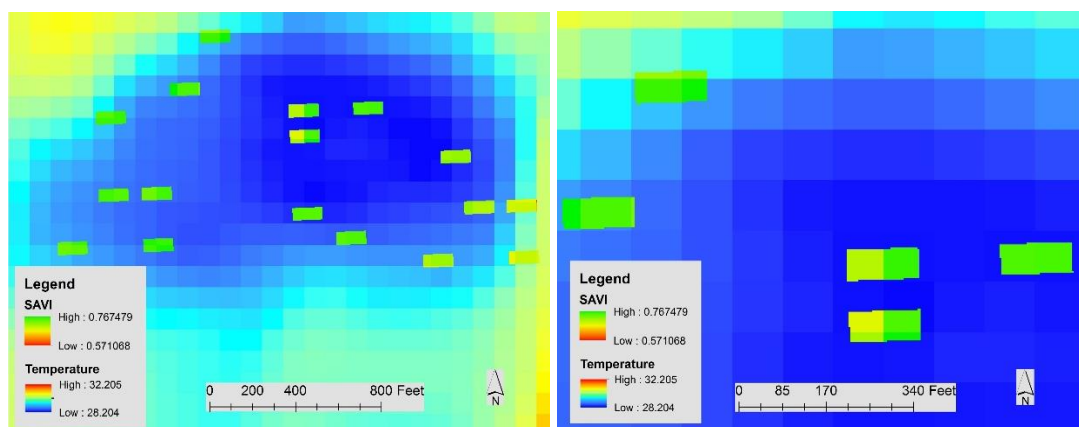


Figure 2.4. Computed SAVI using Landsat 8 imagery for experimental plots (green and yellow) with a Landsat 8 thermal infrared surface temperature image background (a) zoomed out view (b) zoomed in view.

imagery used a ground resolution of about 1m. The enhanced resolution was useful for studying spatial variability closely as depicted in figure 2.4 (b). The UAS thermal infrared image clearly demarcates an area of high temperatures which crosses some parts of the plots. This could help identify field characteristics more precisely and consequently, help to make better prescription maps for VRI. The minimum SAVI value presented in Figure 2.3 was 0.3, which was much lower than lowest SAVI value for the Landsat case. The maximum computed SAVI values in both Landsat and UAS (0.77 for both Landsat and UAS) cases were similar. The relatively coarse Landsat resolution smooths the effect of high temperature areas with adjacent cool areas, making it more difficult to study variable field characteristics.

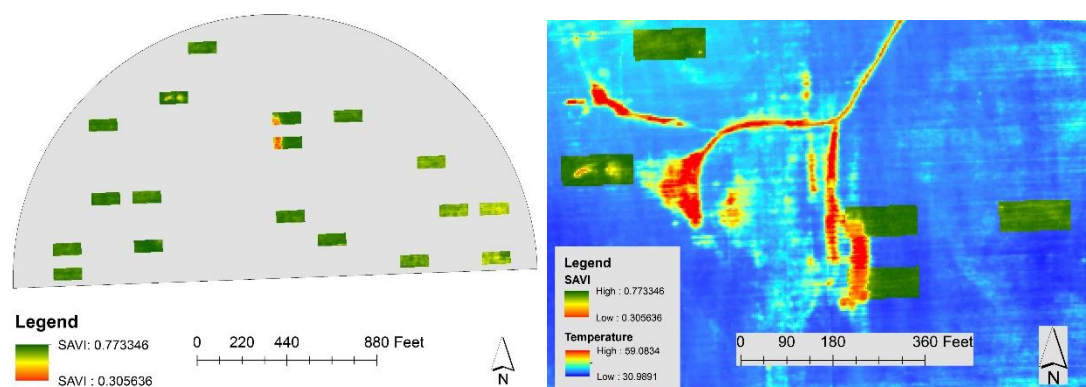


Figure 2.5. Computed SAVI using UAS imagery for experimental plots (green and red) with a UAS thermal infrared surface temperature image background (a) zoomed out view (b) zoomed in view.

2.3.8.2 Temporal Resolution

Landsat 7 and 8 pass over a location every 16 days with an offset of 8 days between the two satellites. The frequency may be sufficient for irrigation scheduling purposes. Landsat images were not usable in the model on days of high cloud cover. In

the study for year 2018, no cloud free Landsat images were acquired from the mid-to-late season. Another issue with using Landsat 7 is missing data for strips in the imagery from the scan line correction problem (USGS, 2018). Missing data in these images was the reason for excluding imagery in the study.

The problem of missing data could be addressed by using a UAS to capture remote sensing images. The UAS can be flown to capture imagery on sunny and calm days (Maguire 2018). The UAS data collection was successful for year 2018 and images were collected for most weeks during the growing season. This promising aspect of UAS imagery could be utilized for reliable VRI management.

2.3.9 Challenges in Using UAS Thermal Infrared Imagery in the TSEB Model

2.3.9.1 Updated Relations for Computing TSEB Parameters

SETMI used relationships as mentioned in Barker et al. (2018b) for computing parameters for TSEB, including fraction of cover, plant height, and leaf area index. These coefficients are applicable for Landsat imagery and are specific to crops. New relationships have been developed for UAS imagery (Maguire 2018). Future work is required to validate TSEB *ET* using UAS imagery with ground truth data from a direct *ET* measurement, such as eddy covariance flux *ET* data.

2.3.9.2 Thermal Infrared Imagery Calibration

Thermal imagery from the UAS was not used in the SETMI model due a need for higher accuracy in canopy temperature when calculating ET with an energy balance. Ongoing efforts are underway to reliably calibrate UAS thermal imagery (Mitch Maguire,

personal communication). A few methods of calibration are discussed in Maguire, 2018, but each one has its own limitations. Future work needs to be done to develop a good methodology to precisely calibrate UAS thermal infrared imagery. In this study, point measurements of mounted Apogee SI-111 infrared thermometers (Apogee, 2018) were compared to respective pixels in the UAS-collected thermal infrared imagery. The mounted infrared thermometers were installed in 12 different locations in the field. A comparison of temperatures obtained from the mounted sensors and respective pixels of the UAS imagery was done. The comparison showed that temperature from mounted sensors was lower than imagery in a majority of cases. The difference between two temperatures was averaged on image dates and used to adjust the respective thermal infrared images through mean adjustment. Table A.4 is a list of temperature measurements from the infrared thermometers and thermal imagery from the UAS at the different sensor locations.

Ongoing work for calibration of thermal imagery and updating physiological relationships for different crops in the model seems to promise use of thermal infrared imagery from UAS into the model in coming years.

2.4 Summary and Conclusions

A field study of VRI was conducted at a field producing maize and soybean in eastern Nebraska. VRI was evaluated on the basis of pumpage reductions and yield potential. Rainfed and uniform irrigation treatments were included along with VRI treatments in the study. VRI was managed with the SETMI model, including a hybrid of two remote sensing-based models, using Landsat in 2017 and 2018. A new VRI treatment

introduced in 2018 included use of K_{cbrf} based water balance model with UAS multispectral imagery. VRI treatments were compared with uniform, and rainfed treatments in terms of crop yield and water response.

In 2017, significantly lower maize yield was observed in the rainfed treatment than both VRI-L and uniform 2 treatments. Mean yields ranged from 11.6 Mg ha⁻¹ to 12.3 Mg ha⁻¹ for maize. The increase in yields in irrigated treatments versus rainfed crop was attributed to irrigation. For soybean, mean yield ranged from 4 Mg ha⁻¹ to 4.1 Mg ha⁻¹. No yield increases were found for soybean due to irrigation applications. In 2018, no significant yield differences were found among treatments for maize and soybean. In 2017, *IWUE* was highest for the uniform 2 treatment (9.3 kg ha⁻¹ mm⁻¹) and lowest for the uniform treatment (6.6 kg ha⁻¹ mm⁻¹) in maize. *IWUE* in soybean was positive only for uniform treatment (0.2 kg ha⁻¹ mm⁻¹). In 2018, *IWUE* was positive only for the uniform treatment (0.1 kg ha⁻¹ mm⁻¹) for maize crop. For soybean, positive *IWUE* was observed for VRI-L (0.5 kg ha⁻¹ mm⁻¹) and VRI-U (0.6 kg ha⁻¹ mm⁻¹).

I_p was different among uniform and VRI treatments for soybean in 2017. I_p for VRI-L treatment (76 mm) was significantly higher than uniform treatment (51 mm). Significant differences were not found for maize. Mean I_p for maize is 77 mm for VRI treatment and 76 mm for uniform treatment. In 2018, VRI-L had lower I_p than other irrigated treatments in soybean. I_p was not significantly different between uniform and VRI-U in maize. It is evident that the VRI treatments were able to produce adequate yields as compared with the uniform treatment and VRI-L performed significantly better than the rainfed treatment for maize in 2017. We found a significant reduction in I_p for

VRI-L treatment in soybean in 2018. Hence, significant water withdrawal reduction was observed for one case in the study.

The higher temporal and spatial resolution of UAS imagery compared to Landsat imagery was beneficial for modeling with newer and finer imagery. The VRI-U treatment managed using multispectral UAS imagery produced yield similar to other treatments and used similar mean irrigation depth compared to the uniform treatment. This signifies that VRI-U could adequately manage irrigation and there is scope of improving modeling using UAS imagery for future. While UAS thermal imagery is often used to identify relative patterns in canopy temperature, using UAS to determine accurate temperatures for surface energy balance modeling remains a challenge. Overall, VRI using SETMI could be adopted for irrigation management to produce adequate yields in sub-humid climates with a reduction in water withdrawals in some scenarios. Further studies are required to implement VRI more accurately and present benefits of VRI.

Acknowledgements

The funding was provided by Graduate Student Support from the Robert B. Daugherty Water for Food Global Institute at the University of Nebraska, a USGS 104(b) grant from the Nebraska Water Center, and a grant from the USDA NIFA Agricultural and Food Research Initiative (Award Number 2017-67021-26249). Additional support was received from the Hatch Act (USDA NIFA, Accession Number 1009760) and the Department of Biological Systems Engineering at the University of Nebraska-Lincoln. I thank Mr. Mark Schroeder and his team from the University of Nebraska's Eastern Nebraska Research and Extension Center for their cooperation and help with field

operations. I also thank Alan Boldt, Mitch Maguire, Jasreman Singh, Isabella Possignolo Presotto, Julienne Irihose, Rene Francis Simbi Mvuyekure, Troy Nelson, Joviale Uwase, and Tonny Ruhinda for their help in collecting data and field work. We also acknowledge personnel from the Biological Systems Engineering Department at University of Nebraska for their support and help throughout the experiment.

2.5 References:

- Allen, R. G., & Wright, W. C. (2002). Conversion of Wright (1981) and Wright (1982) Alfalfa-Based Crop Coefficients for Use with the ASCE Standardized Penman-Monteith Reference Evapotranspiration Equation. *Technical Note-USDA-ARS, Kimberly, Id.*,
- Barker, Burdette. (2017). Spatial Irrigation Management Using Remote Sensing Water Balance Model and Soil Water Content Monitoring. University of Nebraska-Lincoln
- Barker, J. B., Heeren, D. M., Neale, C. M. U., & Rudnick, D. R. (2018a). Evaluation of Variable Rate Irrigation Using a Remote-Sensing-Based Model. *Agricultural Water Management*, 203 63–74. doi:10.1016/j.agwat.2018.02.022
- Barker, J. B., Neale, C. M. U., Heeren, D. M., & Suyker, A. E. (2018b). Evaluation of a Hybrid Reflectance-Based Crop Coefficient and Energy Balance Evapotranspiration Model for Irrigation Management. *Transactions of the ASABE*, 61(2), 533–48
- Barsi, J. A., Barker, J. L., & Schott, J. R. (2003). An Atmospheric Correction Parameter Calculator for a Single Thermal Band Earth-Sensing Instrument. In *IEEE International Geoscience and Remote Sensing Symposium 2003*, 2–4.

doi:10.1109/IGARSS.2003.1294665

Bausch, W. C., & Neale, C. M. U. (1987). Crop Coefficients Derived from Reflected Canopy Radiation : A Concept. *Transactions of the ASAE*, 30(3), 703–9.

Campos, Isidro, Neale, Christopher M.U., Suyker, Andrew E., Arkebauer, Timothy J., & Gonçalves, Ivo Z. (2017). Reflectance-Based Crop Coefficients REDUX: For Operational Evapotranspiration Estimates in the Age of High Producing Hybrid Varieties. *Agricultural Water Management*, 187 140–53.

doi:10.1016/j.agwat.2017.03.022

Daccache, A., Knox, J. W., Weatherhead, E. K., Daneshkhah, A., & Hess, T. M. (2015). Implementing Precision Irrigation in a Humid Climate - Recent Experiences and on-Going Challenges. *Agricultural Water Management*, 147 135–43.

doi:10.1016/j.agwat.2014.05.018

Djaman, K., & Irmak, S. (2012). Soil Water Extraction Patterns and Crop, Irrigation, and Evapotranspiration Water Use Efficiency of Maize Under Full and Limited Irrigation and Rainfed Settings. *Transactions of the ASABE*, 55(4), 1223–38.

doi:10.13031/2013.42262

Evans, R. G., LaRue, J., Stone, K. C., & King, B. A. (2013). Adoption of Site-Specific Variable Rate Sprinkler Irrigation Systems. *Irrigation Science*, 31(4), 871–87.

doi:10.1007/s00271-012-0365-x

Geli, H. M. E., & Neale, C. M. U. (2012). Spatial EvapoTranspiration Modelling Interface (SETMI). In *Remote Sensing and Hydrology*, 171–74.

- Irmak, S., Odhiambo, L. O., Specht, J. E., & Djaman, K. (2013). Hourly and Daily Single and Basal Evapotranspiration Crop Coefficients as a Function of Growing Degree Days, Days After Emergence, Leaf Area Index, Fractional Green Canopy Cover, and Plant Phenology for Soybean. *Transactions of the ASABE*, 56(5), 1785–1803. doi:10.13031/trans.56.10219
- Johnson, B., Thompson, C., Giri, A., & NewKirk, S. V. (2011). Nebraska Irrigation Fact Sheet. *Report No. 190*. Available online: http://agecon.unl.edu/c/document_library/get_file?uuid=a9fcd902-4da9-4c3f-9e04-c8b56a9b22c7&groupId=2369805&.pdf
- Lo, T., Heeren, D. M., Martin, D. L., & Mateos, L. (2016). Pumpage Reduction by Using Variable Rate Irrigation to Mine Undepleted Soil Water. *Transactions of the ASABE*, 59(5), 1285–98. doi:10.13031/trans.59.11773
- Maguire, Mitch. (2018). An Evaluation of Unmanned Aerial System Multispectral and Thermal Infrared Data as Information for Agricultural Crop and Irrigation Management. University of Nebraska-Lincoln.
- Miller, K. A., Luck, J. D., Heeren, D. M., Lo, T., Martin, D. L., & Barker, J. B. (2017). A Geospatial Variable Rate Irrigation Control Scenario Evaluation Methodology Based on Mining Root Zone Available Water Capacity. *Precision Agriculture*, 19(4), 666. doi:10.1007/s11119-017-9548-z
- NASA. (2018). Landsat 8. Accessed November 18, 2018. Retrieved from <https://landsat.gsfc.nasa.gov/landsat-data-continuity-mission/>

- Neale, C. M. U., Bausch, W. C., & Heerman, D. F. (1989). Development of Reflectance-Based Crop Coefficients for Corn. *Transactions of the ASAE*, 32(6), 1891–99.
- Neale, C. M.U., Geli, H. M.E., Kustas, W. P., Alfieri, J. G., Gowda, P. H., Evett, S. R., Prueger, J. H., et al. (2012). Soil Water Content Estimation Using a Remote Sensing Based Hybrid Evapotranspiration Modeling Approach. *Advances in Water Resources*, 50 152–61. doi:10.1016/j.advwatres.2012.10.008
- Norman, J. M., Kustas, W. P., & Humes, K. S. (1995). Source Approach for Estimating Soil and Vegetation Energy Fluxes in Observations of Directional Radiometric Surface Temperature. *Agricultural and Forest Meteorology*, 77(3–4), 263–93. doi:10.1016/0168-1923(95)02265-Y
- O’Shaughnessy, S. A., Evett, S. R., Andrade, M. A., Workneh, F., Price, J. A., & Rush, C. M. (2016). Site-Specific Variable-Rate Irrigation as a Means to Enhance Water Use Efficiency. *Transactions of the ASABE*, 59(1), 239–49. doi:10.13031/trans.59.11165
- Raes, D., P. Steduto, T. C. Hsiao, and E. Fereres. 2017. “Chapter 3: Calculation Procedures.” *AquaCrop Version 6.0 Reference Manual*. March 2017. Food and Agriculture Organization of the United Nations, Rome, Italy.
- Schaible G, Aillery M. 2015. Irrigation and water use. <http://www.ers.usda.gov/topics/farm-practices-management/irrigation-water-use.aspx>. Accessed on 3 February 2015.
- SCS. (1985). *Part 630 Hydrology National Engineering Handbook Chapter 10*

Estimation of Direct Runoff from Storm Rainfall

- Shelton, D. P., & Jasa, P. J. (2009). Estimating Percent Residue Cover Using the Line-Transect Method. *NebGuide*, 1–3
- Soil Survey Staff. (2018). Web Soil Survey. Retrieved from <http://websoilsurvey.sc.egov.usda.gov/App/HomePage.htm>
- Stone, K. C., Bauer, P. J., Busscher, W. J., Millen, J. A., Evans, D. E., & Strickland, E. E. (2015). Variable-Rate Irrigation Management Using an Expert System in the Eastern Coastal Plain. *Irrigation Science*, 33(3), 167–75. doi:10.1007/s00271-014-0457-x
- Stone, K. C., & Sadler, E. J. (2016). Assessing Spatial Variation of Corn Response To Irrigation Using a Bayesian Semiparametric Model. *Transactions of the ASABE*, 59(1), 251–61. doi:10.13031/trans.59.10942
- Sui, R., & Yan, H. (2017). Field Study of Variable Rate Irrigation Management in Humid Climates. *Irrigation and Drainage*, 66(3), 327–39. doi:10.1002/ird.2111
- USGS. (2018). SLC-off Products: Background. Accessed November 18, 2018. Retrieved from <https://landsat.usgs.gov/slc-products-background>
- William L. Kranz, James E. Specht. (2012). Irrigating Soybean. *NebGuide*,. <http://extensionpublications.unl.edu/assets/pdf/g1367.pdf>
- Yonts, C.D., Melvin, S.R., & Eisenhower, D.E. (2008). Predicting the Last Irrigation of the Season. *NebGuide*, G1871.

CHAPTER 3. GENERAL OBSERVATIONS AND FUTURE WORK

3.1 Seasonal Depletion for Sample Plots in VRI and Uniform Treatments

This section discusses how various inputs in model changed root zone depletion for plots under different treatment. Figure 3.1 and 3.2 shows seasonal soil water depletion for a plot in uniform and VRI-L treatment, respectively. Rain and precipitation events are shown at bottom of figure with orange and blue spikes. The dark blue in the figure depicts the seasonal root zone depletion. These graphs were computed from 2017 season. In the uniform treatments, model was periodically adjusted using soil water content measurements from NP. In most scenarios, the soil water measurement decreased the depletion in the model. In other words, measured depletion was lower than modeled depletion in most cases. This adjustment reduced model drift that was observed in Barker et al. (2018a).

Seasonal soil water depletion in VRI plot is depicted using figure 3.2. This depletion was adjusted on days of NP measurement and acquisition of remote sensing imagery. The thermal infrared imagery was used to run TSEB, which was used to detect stress in crop root zone. The TSEB adjustment updated the soil water balance, usually by increasing the modeled root zone depletion.

In figure 3.2, the TSEB usually resulted in relatively small updates to the soil water balance; however, depletion was increased by 50 mm on 30 June, 2017. The TSEB *ET* input on this date in the model mainly caused the large increase in depletion. TSEB *ET* on this date was calculated lower than water balance *ET* which indicated water stress. This corresponded to the stress coefficient term in the crop coefficient decreasing

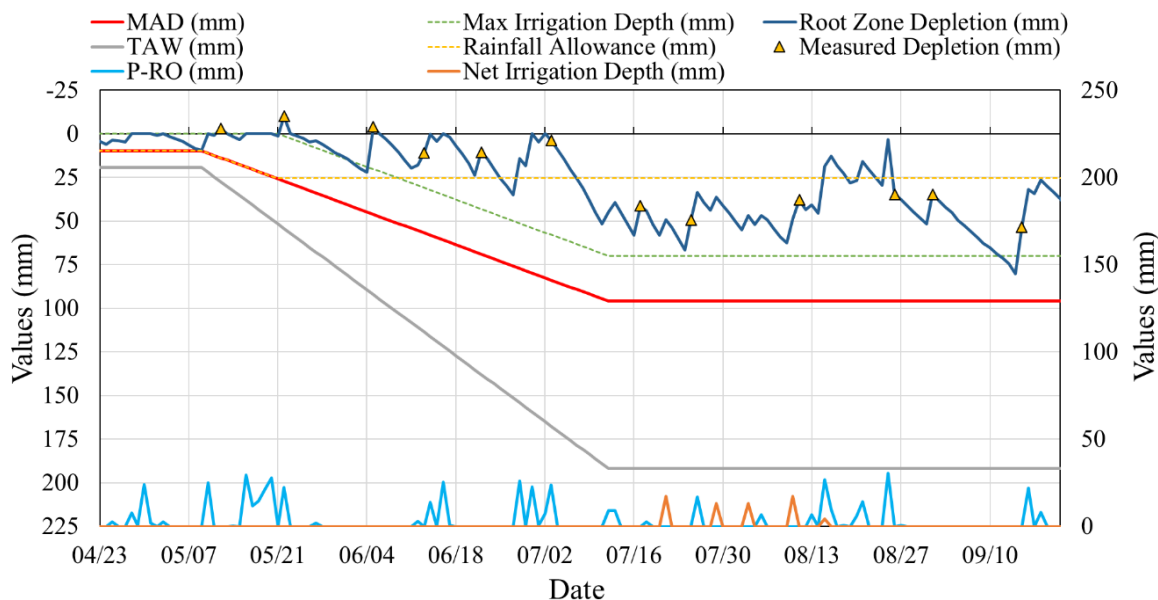


Figure 3.1. Seasonal soil water depletion for a uniform plot for ENREC Maize in 2017. Maximum irrigation depth is shown by green dotted line taking reference to MAD (red line).

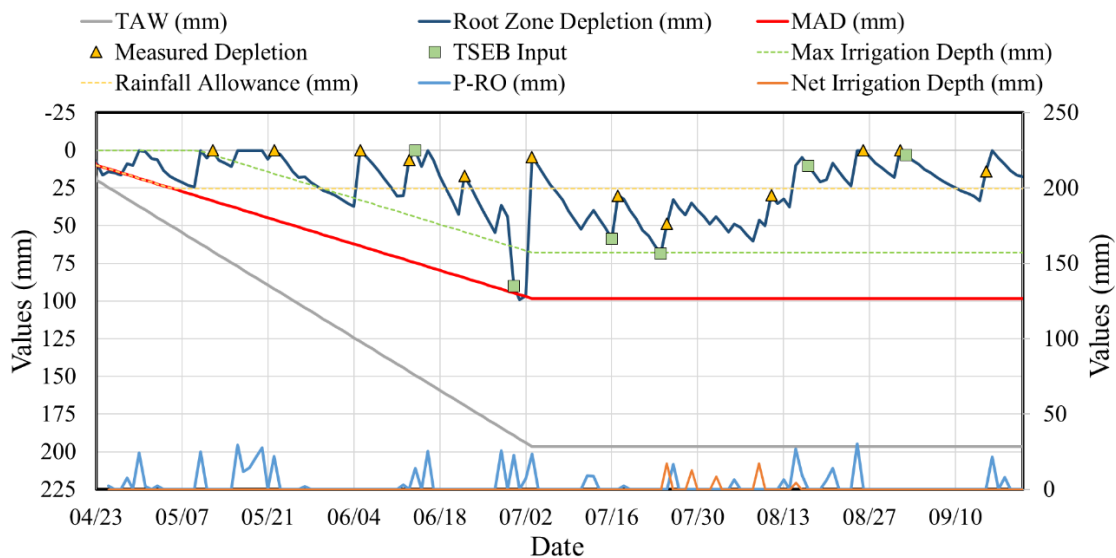


Figure 3.2. Seasonal soil water depletion for a VRI plot for ENREC Maize in 2017. Maximum irrigation depth is shown by green dotted line taking reference to MAD (red line).

(i.e. less than 1). The lower TSEB *ET* could possibly be a result of a high temperature thermal image compared to ambient air temperature on this day. Conversely on 3 July,

2017, the depletion decreased to reach field capacity. This was result of both wetting of soil profile by soil water content measurements on 3 July and rain events happening between 30 June and 3 July.

3.2 Catch Can Test for System Evaluation

We conducted catch can test at the end of 2017 growing season. The pivot was run in a full VRI mode with VRI prescription. The cans were laid out in a grid with spacing of 10 feet between adjacent cans. The pivot road was used to lay cans along the lateral pipe of center pivot and cans were also set perpendicular to the pivot road to capture efficiencies when prescription depth is changed from a zone to another. Figure 3.3 shows catch can layout and prescription map for the test. The test was done on 3 November, 2017.

The measured depth of water in catch cans was positively correlated with prescribed irrigation depth showing promising results. Average percentage difference between measured and prescribed irrigation depth was approximately 25 %. The percentage difference was calculated using:

$$\% \text{ difference} = \frac{(\text{prescribed irrigation depth} - \text{measured depth in cans})}{\text{Prescribed irrigation depth}} * 100$$

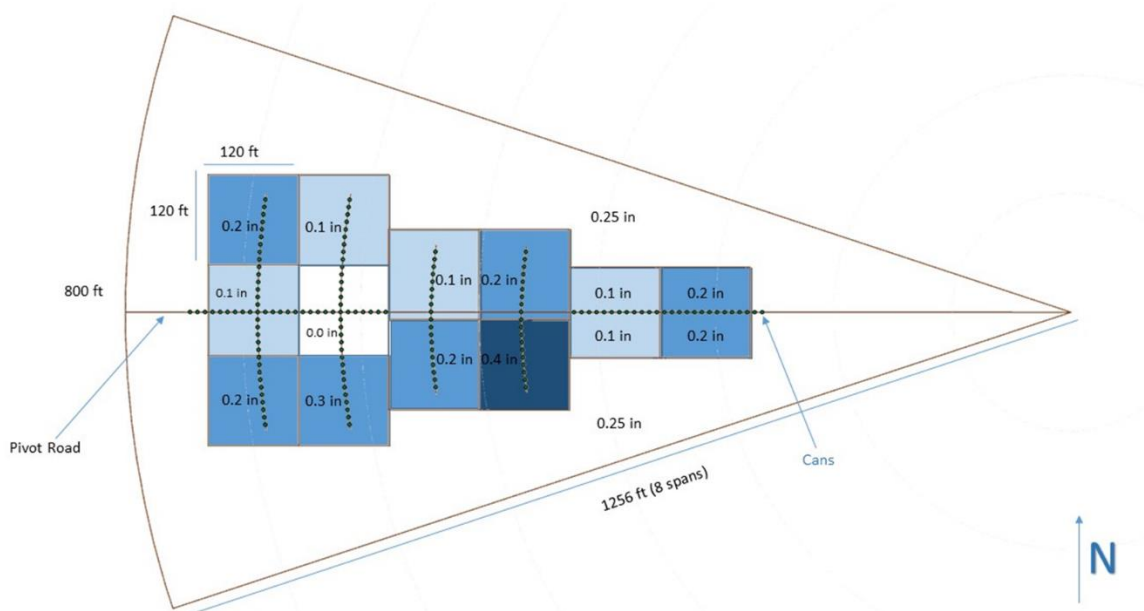


Figure 3.3. Catch can layout (shown in dots) and irrigation prescription map for conducting end of season catch can evaluation in 2017.

3.3 Future Direction and Recommendations

The study of VRI management using spatial *ET* model could be improved by implementing points discussed in this section. Plots were randomized using soil blocks based on *AWC*. Treatments were randomly assignment to different blocks. It was observed in the spatial yield maps and plot yield numbers that there were more factors that may have affected the yield. These could be topography, soil type, or nutrient availability in soils. Consideration of factors like historic yield maps, additional soil properties like apparent electrical conductivity, topography etc. while treatment assignment to different experimental plots could prove beneficial. This will help to remove effects from unknown variables in the results by distributing the variation equally among treatments. Additionally, areas where crop does not perform well, areas with

frequent flooding or excessive residue cover, as was observed in this study, should be avoided. These areas create bias for some treatments and could affect results.

Conclusively, analyzing historic yield maps can help identify different field characteristics and can help effectively design the study without any bias in any specific treatment.

Perhaps it is important to determine a more optimum size of experimental plots for the study, especially in large scale studies. To compute the results for this study, raw results at higher resolution were scaled up to experimental plots size. Scaling up of results with mean value may smoothen any spatial patterns that may be present in raw results. This can cause significant results to be non-significant. Hence, defining appropriate plot size is essential to observe significant results between treatments.

Adjustment with soil water content measurements helped improve the model accuracy for simulating root zone depletion. We used mean adjustment using soil water monitoring at 4 locations. This adjustment was sufficient to improve the model and create precise prescriptions. However, spatial adjustment for water content would be leap for the study. This could be possible by correlating the thermal infrared image collected from UAS with point source soil water measurements. The correlation could be used to spatially adjust the modeled depletion, which could be a potential improvement over mean adjustment over the entire image used in the study. It has to be determined whether surface soil water content could be a good parameter to compare with thermal temperature of the image or deeper soil water contents should also be taken into consideration when comparison is made.

The TSEB model using UAS imagery was not ready to be used for adjusting *ET* on remote sensing imagery collection dates. This requires considerable efforts before TSEB *ET* could be included in creating VRI prescriptions. Detailed challenges for the use of TSEB *ET* is discussed in section 3.4. Future work needs to be conducted in this direction to be confident about using TSEB *ET* using UAS imagery.

Deep percolation methodology used in our study, in general, could be regarded as an improvement over Barker et al. (2018a) methodology. The improvement in the model was led by B. Barker and used in 2018 UAS imagery treatments. The new methodology allowed soil water content to increase more than FC and reach up to saturation. The soil water content higher than FC could now be utilized for evapotranspiration, which was not possible earlier. Since, this addition was made in 2018 growing season, more evaluation needs to be done to study accuracy of this methodology. This methodology also resulted in lower *DP* due to water being utilized for evapotranspiration.

A. APPENDIX:

A.1 Modeling Accuracy Using the New Method of Deep Percolation Estimation

In this section, accuracy of the model when using different methods of estimating seasonal depletion, will be discussed. Two methods were different in terms of estimation of DP between NP days. The first method used the instantaneous drainage method (DP_i), where in cases of soil water content present above FC was drained at end of the day. Second method included a decaying function for estimation of DP (DP_d). This allowed soil water content above FC to drain slowly and be used for ET . Water balance was run using these two methods and model drift in each case was calculated using measured NP depletion. Model drift was referred to the difference between measured depletion from NP and modeled depletion. Soil water content measurements corrected model on NP measurement days. Root zone used for these model runs was 1.22 m.

Two plots in both crops each were selected to model depletion throughout season in 2017. In summary, two plots in two crops each and using two different model runs were compared. Sum of modeled root zone depletion (D_{mo}) and measured root zone depletion (D_{ms}) at NP measurement days were computed. The difference of these depletions was used as a measure to describe model accuracy. This difference was computed for all four selected plots.

The plots were chosen from different soil groups. Table A.1 provides the sum of modeled and measured depletion on NP measurement days. Difference could be used as a measure to determine closeness of simulated depletion to measurement. In each case, difference was smaller for decaying DP method. This implied that use of decaying DP

method improved the ability to model depletion. Figure A.1. shows how D_{ms} and D_{mo} were simulated throughout the season and their closeness to NP measured depletions. DP events happened early in the season where different modeled depletion values can be observed. Later in the season, there is no difference between modeled depletion values because of no DP events.

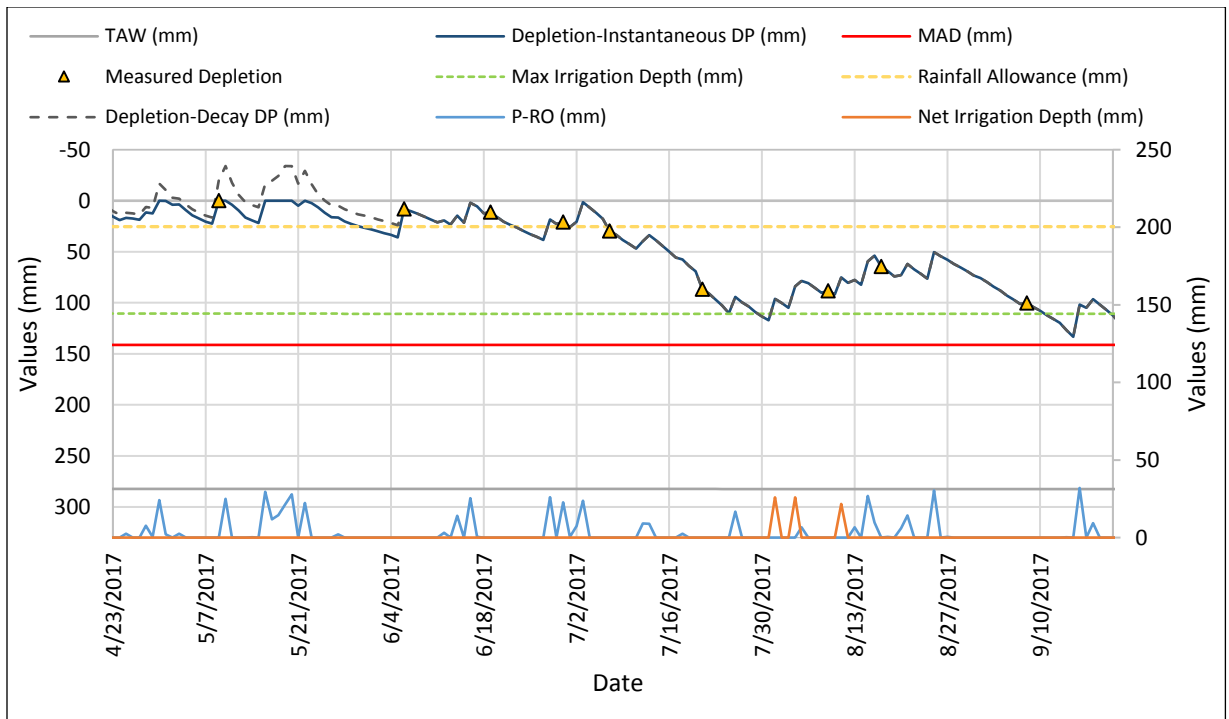


Figure A.1. Seasonal depletion modeled using instantaneous and decaying deep percolation (DP) methods for one plot in soybean in 2017.

Table A.1. Comparison of two methods of simulating seasonal modeled depletion using measured depletion.

	Σ seasonal D_{ms} (mm)	Σ seasonal D_{mo} (mm)	$\Sigma D_{mo} - \Sigma D_{ms}$ (mm)
<i>Plot 1 Maize 2017</i>			
Instantaneous <i>DP</i>	585.2	602.7	17.5
Decaying <i>DP</i>	585.2	584.1	-1.1
<i>Plot 2 Maize 2017</i>			
Instantaneous <i>DP</i>	446.8	558.9	112.1
Decaying <i>DP</i>	446.8	512.8	66
<i>Plot 3 Soybean 2017</i>			
Instantaneous <i>DP</i>	435.9	531.3	95.4
Decaying <i>DP</i>	435.9	513.6	77.7
<i>Plot 4 Soybean 2017</i>			
Instantaneous <i>DP</i>	385.6	537.5	151.9
Decaying <i>DP</i>	385.6	513.6	128

A.2 Spatial Variability in Depletion Among Plots

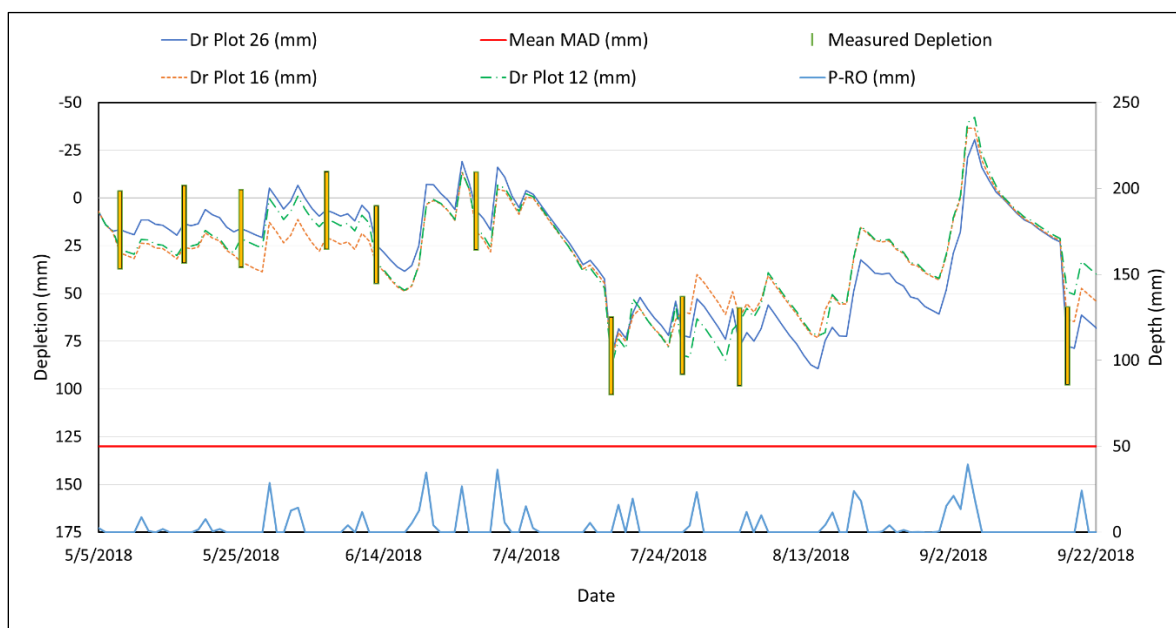


Figure A.2. Seasonal depletion for 3 plots in VRI-U for soybean in 2018. These three plots belong to different soil blocks (6 blocks for north half plots). Mean manageable allowable depletion of these 3 plots is depicted with red line. All values except net rainfall amount (P-RO) is plotted on left y-axis in reverse direction. Plot 12, 16 and 26 were prescribed with total gross irrigation of 117, 91 and 107 mm. Plot 12, 16 and 26 had mean dry yield of 3.8, 3.1 and 3.1 ($Mg\ ha^{-1}$). Depletion for these 3 plots vary from each other throughout season and indicates the variability in irrigation management.

A.2 Tables and Figures

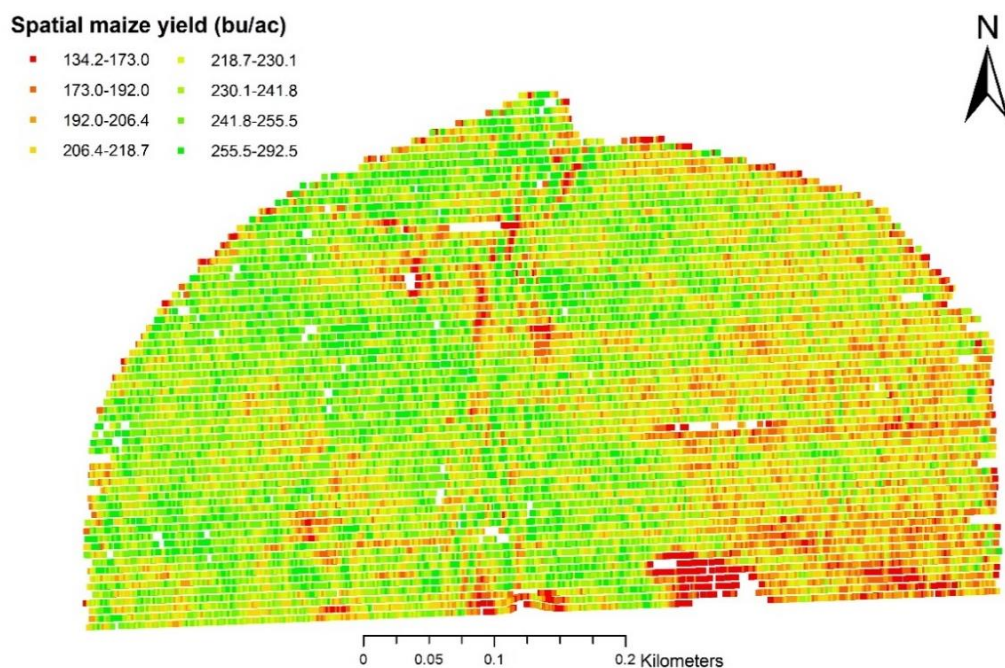


Figure A.3. Spatial maize yield (bu ac⁻¹) at market moisture planted north of the field in 2017.

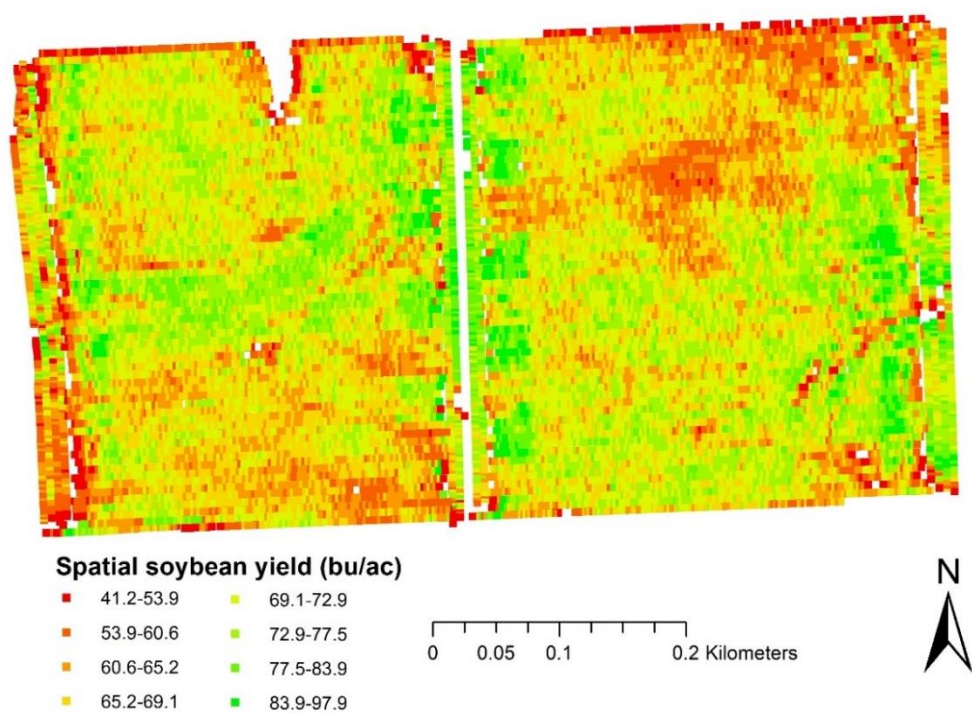


Figure A.4. Spatial soybean yield (bu ac⁻¹) at market moisture in south of the field in 2017.

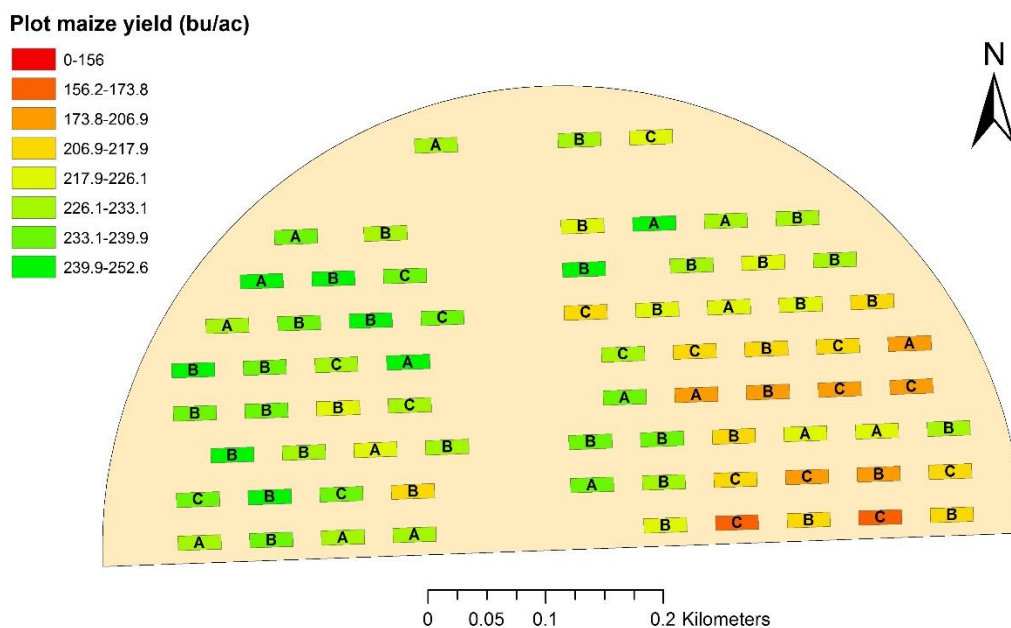


Figure A.5. Plot maize yield (bu ac^{-1}) at market moisture planted north of the field in 2017. A denotes treatment VRI-L, B denotes treatment uniform 2, C denotes treatment uniform, and D denotes treatment rainfed.

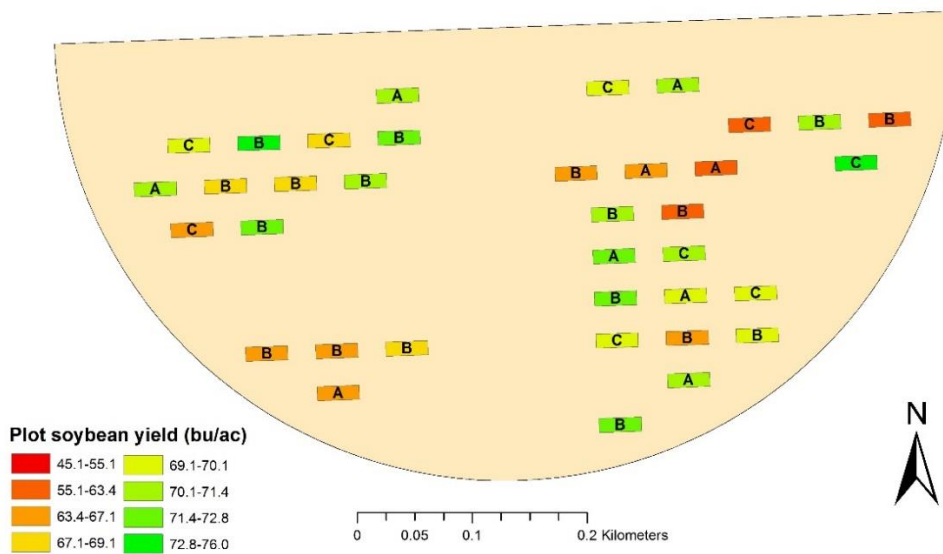


Figure A.6. Plot soybean yield (bu ac^{-1}) at market moisture planted south of the field in 2017. A denotes treatment VRI-L, B denotes treatment uniform 2, C denotes treatment uniform, and D denotes treatment rainfed.

Table A.2. Summary of multivariate analysis of variance (MANOVA) tests using Wilks's Lambda Statistic in 2017 and 2018.

Site Crop Year	Effect	Wilks' Lambda	F Value	Num DF	Den DF	Pr > F
<i>Maize 2017</i>	Treatment	0.13	14.9	12	153.7	<.0001
	Blocking	0.41	3.0	20	193.3	<.0001
<i>Soybean 2017</i>	Treatment	0.03	15.8	12	71.7	<.0001
	Blocking	0.54	2.4	8	54	0.0265

Table A.3. Summary of univariate analysis of variance (ANOVA) tests for various response variables for all fields in 2017

Var	Effect								
		Num DF	Den DF	F Value	Pr > F	Num DF	Den DF	F Value	Pr > F
<i>Maize 2017</i>						<i>Soybean 2017</i>			
<i>ET_a</i>	Trt	3	61	57.03	< 0.0001	3	30	9.55	0.0001
	Block	5	61	4.34	0.0019	2	30	0.7	0.0187
<i>DP</i>	Trt	3	61	0.33	0.8059	3	30	0.68	0.5704
	Block	5	61	8.04	< 0.0001	2	30	6.14	0.0058
<i>ΔSW</i>	Trt	3	61	3.39	0.0235	3	30	0.88	0.4648
	Block	5	61	4.31	0.002	2	30	0.48	0.6225
Yield	Trt	3	61	3.12	0.0325	3	30	0.17	0.918
	Block	5	61	1.04	0.4035	2	30	0.21	0.8096

Table A.4. Temperature (°C) of thermal imagery from UAS and temperature measurements from IRT for 29 date-locations in the field.

Location	Date	UAS Temp (°C)	IRT Temp (°C)	UAS – IRT Temp (°C)
1	July 2, 2018	25.6	27.6	-2
2	July 2, 2018	29.6	27.1	2.5
3	July 2, 2018	27.8	27.4	0.4
4	July 2, 2018	28.9	28.1	0.8
5	July 2, 2018	31.1	27.4	3.7
6	July 2, 2018	30.9	31.6	-0.7
7	July 2, 2018	34.9	30.6	4.3
8	July 2, 2018	35.4	29.2	6.2
9	July 2, 2018	29.3	29.6	-0.3
10	July 6, 2018	26.4	27.5	-1.1
11	July 6, 2018	26.2	28.3	-2.1
12	July 6, 2018	26.6	27.3	-0.7
1	July 6, 2018	25.6	27.2	-1.6
2	July 6, 2018	28.5	27.8	0.7
3	July 6, 2018	30.1	29.6	0.5
4	July 6, 2018	29.2	29.9	-0.7
5	July 6, 2018	28.7	27.8	0.9
6	July 6, 2018	28.1	28.5	-0.4

7	July 11, 2018	31.2	32	-0.8
8	July 11, 2018	33	30.4	2.6
9	July 11, 2018	32.3	30.4	1.9
10	July 11, 2018	33.3	30.7	2.6
11	July 11, 2018	32.4	30.6	1.8
12	July 11, 2018	31.8	31.1	0.7
1	July 11, 2018	33.8	34.6	-0.8
2	July 11, 2018	32.7	31.2	1.5
3	July 11, 2018	31.6	30.5	1.1
4	July 11, 2018	32.1	30.9	1.2
5	July 11, 2018	32	30.2	1.8